iScience

CellPress
OPEN ACCESS

Article

Dysfunctional EGFR and oxidative stress-induced PKD1 signaling drive formation of DCLK1+ pancreatic stem cells

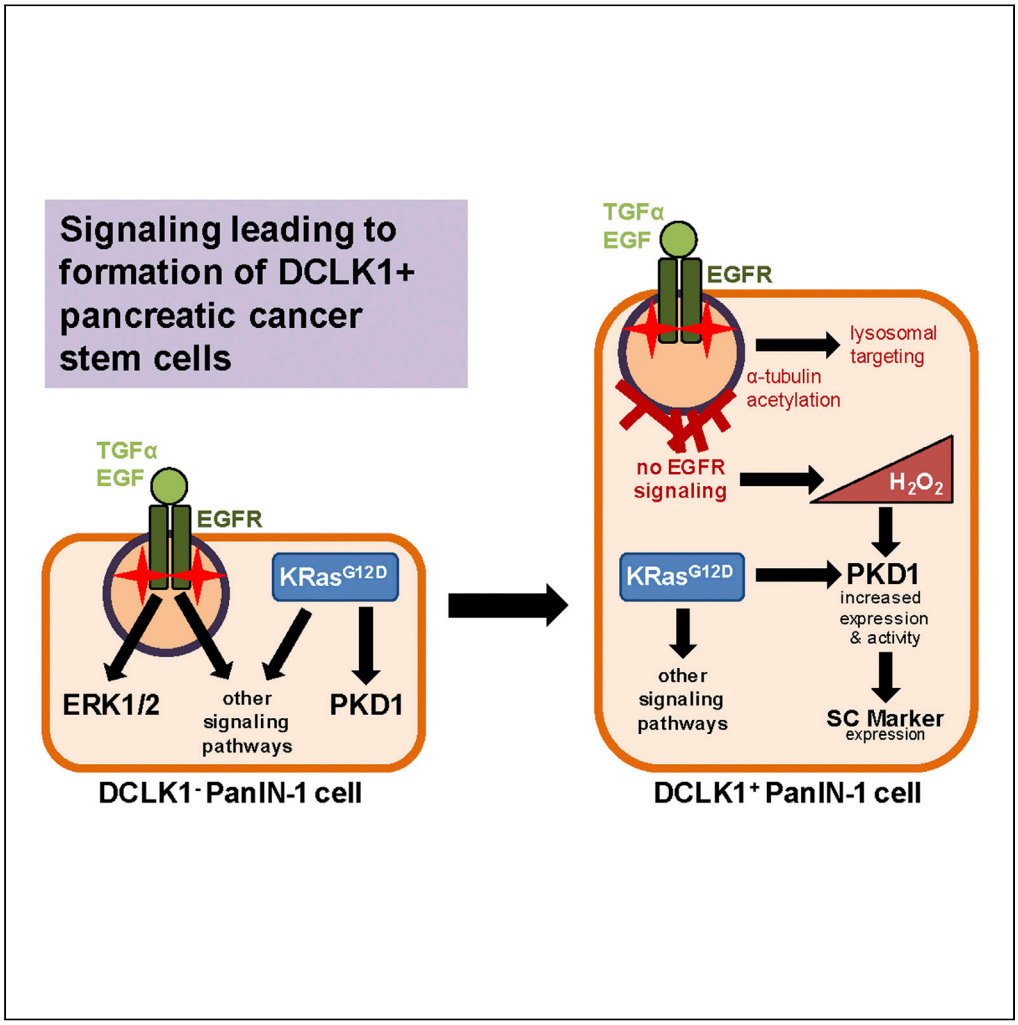

Figure360▷ For a Figure360 author presentation of this figure, see https://doi.org/10.1016/j.isci.2020.102019.

Alicia K. Fleming Martinez, Heike R. Döppler, Ligia I. Bastea, ..., Michael Leitges, Geou-Yarh Liou, Peter Storz

storz.peter@mayo.edu

HIGHLIGHTS

DCLK1+ PanIN cells have abrogated EGFR signaling and increased oxidative stress

Inhibition of EGFR signaling increases DCLK1+ cells, oxidative stress, and PKD1

PKD1 contributes to the abundance of DCLK1+ stem cells in PanIN lesions

Stem cell markers, including OCT4 and CD133, are increased by PKD1

Fleming Martinez et al., iScience 24, 102019 January 22, 2021
https://doi.org/10.1016/j.isci.2020.102019

iScience

CellPress
OPEN ACCESS

Article

Dysfunctional EGFR and oxidative stress-induced PKD1 signaling drive formation of DCLK1+ pancreatic stem cells

Alicia K. Fleming Martinez,[1] Heike R. Döppler,[1] Ligia I. Bastea,[1] Brandy Edenfield,[1] Tushar Patel,[2] Michael Leitges,[3] Geou-Yarh Liou,[4] and Peter Storz[1,5,*]

SUMMARY

Doublecortin-like kinase 1 (DCLK1)-positive pancreatic cancer stem cells develop at a precancerous stage and may contribute to the lack of efficacy of pancreatic cancer therapy. Although PanIN cells express oncogenic KRas and have an increased activity of epidermal growth factor receptor (EGFR), we demonstrate that, in DCLK1$^+$ PanIN cells, EGFR signaling is not propagated to the nucleus. Mimicking blockage of EGFR with erlotinib in PanIN organoid culture or in p48^{cre};Kras^{G12D} mice led to a significant increase in DCLK1$^+$ PanIN cells. As a mechanism of how EGFR inhibition leads to formation of DCLK1$^+$ cells, we identify an increase in hydrogen peroxide contributing to activation of Protein Kinase D1 (PKD1). Active PKD1 then drives stemness and abundance of DCLK1$^+$ cells in lesions. Our data suggest a signaling mechanism that leads to the development of DCLK1$^+$ pancreatic cancer stem cells, which can be exploited to target this population in potential therapeutic approaches.

INTRODUCTION

Pancreatic ductal adenocarcinoma (PDA) has been difficult to target, with a 5-year survival rate of only 9% (Siegel et al., 2020). A key factor in this dismal rate is the presence of cancer stem cells (CSCs), which occur at early stages of tumorigenesis (Qu et al., 2015; Rhim et al., 2012), are resistant to chemotherapy (Gzil et al., 2019; Hermann et al., 2007; Hong et al., 2009), and contribute to tumor recurrence (Vinogradov and Wei, 2012). CSCs have the ability to self-renew and initiate tumors with relatively few cells (Bailey et al., 2014; Gzil et al., 2019; Li et al., 2007), making them essential targets for novel therapeutic approaches.

We here focus on a population of cells with cancer stem cell properties in the pancreas, which is characterized by the expression of Doublecortin-like kinase 1 (DCLK1), a microtubule-associated protein (Lin et al., 2000). These CSCs express, in addition to DCLK1, acetylated α-tubulin (Bailey et al., 2014), β-endorphin (Delgiorno et al., 2014), and the stemness markers CD133 (Bailey et al., 2014), CD24/CD44/ESA (Bailey et al., 2014), and Notch1 (Sureban et al., 2011). Furthermore, DCLK1 in these cells upregulates PD-L1 through the Hippo pathway (Yan et al., 2020), which is implicated in stem cell maintenance (Harvey et al., 2013). Another feature of these cells is the presence of Y1068-phosphorylated epidermal growth factor receptor (EGFR), clustered in an apical region (Delgiorno et al., 2014).

In mouse models for PDA the DCLK1$^+$ population is most abundant in acinar-to-ductal metaplasia (ADM) and pancreatic intraepithelial neoplasia 1A/1B (PanIN-1A/1B) lesions (Bailey et al., 2014; Delgiorno et al., 2014) but is also increased in the serum of patients with stage I and II pancreatic cancer (Qu et al., 2015). Although formed during early tumorigenesis, DCLK1$^+$ lesion cells show *bona fide* CSC properties. For example, they have enhanced clonogenic ability and can initiate tumor formation (Bailey et al., 2014). Moreover, they disseminate early in the KPC (Kras^{G12D};p53^{R172H};Pdx1^{cre}) mouse model for PDA (Qu et al., 2015). Consequently, DCLK1 expression in patient tumors is associated with expression of the cancer stem cell markers CD44/CD24/EpCAM and goes along with shorter median overall survival time, more frequent relapse, and shorter relapse-free survival (Nishio et al., 2017). Thus, understanding the mechanisms driving this malignant cell type is critical to be able to combat pancreatic cancer.

[1]Department of Cancer Biology, Mayo Clinic Comprehensive Cancer Center, Mayo Clinic, Jacksonville, FL 32224, USA

[2]Department of Transplantation, Mayo Clinic Comprehensive Cancer Center, Mayo Clinic, Jacksonville, FL 32224, USA

[3]Division of Biomedical Sciences/Faculty of Medicine, Craig L Dobbin Genetics Research Centre, Memorial University of Newfoundland, St. John's, Newfoundland A1B 3V6, Canada

[4]Department of Biological Sciences, Center for Cancer Research & Therapeutic Development, Clark Atlanta University, Atlanta, GA 30314, USA

[5]Lead contact

*Correspondence: storz.peter@mayo.edu

https://doi.org/10.1016/j.isci.2020.102019

Of the three members of the Protein Kinase D (PKD) family of serine-threonine kinases, Protein Kinase D1 (PKD1) has been identified as a driver of pancreatic cancer initiation (Liou et al., 2015). In KC ($p48^{cre}$;$Kras^{G12D}$) mice, PKD1 drives ADM and progression to PanINs (Liou et al., 2015). In these transformation processes PKD1 acts downstream of oncogenic KRas, which initiates its activation through increasing the generation of reactive oxygen species (ROS) such as hydrogen peroxide (H_2O_2) (Liou et al., 2016). An increase in H_2O_2 mediates phosphorylation of PKD1 at tyrosine residue 95 (Y95), which is a specific marker for ROS-activated PKD1 (Doppler and Storz, 2007). PKD1 has been shown to activate the transcription factors Notch1 and nuclear factor-kB (NF-kB) to drive early metaplasia (Liou et al., 2015, 2016). However, it is unclear if (or how) PKD1 affects the $DCLK1^+$ stem cell population, which has been shown by lineage tracing experiments to develop from $Kras^{G12D}$-expressing ADM or PanIN cells (Bailey et al., 2014).

We here show that, in $DCLK1^+$ PanIN cells, although EGFR is phosphorylated at Y1068, owing to the high presence of acetylated α-tubulin and apical clustering, signaling is not propagated to the nucleus. Inhibition of EGFR signaling, either through this mechanism or through inhibition with erlotinib, leads to a significant increase in $DCLK1^+$ PanIN cells. An increase in hydrogen peroxide as a result of EGFR inhibition contributes to activation of PKD1, which contributes to both occurrence and stemness of $DCLK1^+$ cells. In summary, we here identified key signaling events in $DCLK1^+$ pancreatic cancer stem cells that can be exploited to target this population in potential therapeutic approaches.

RESULTS

EGFR, although autophosphorylated, does not signal downstream to ERK1/2 in $DCLK1^+$ PanIN cells

Expression of DCLK1, acetylated α-tubulin, and β-endorphin characterizes a population of pancreatic cancer stem cells that are formed in low-grade lesions early during tumor development (Bailey et al., 2014; Delgiorno et al., 2014). Lineage tracing experiments showed that these cells develop from $Kras^{G12D}$-expressing ADM or PanIN cells and are distinct to the $DCLK1^+$ Tuft cells that originate in the intestine, but they can also be detected in the pancreas (Bailey et al., 2014; Westphalen et al., 2016). We confirmed previous reports (Bailey et al., 2014; Delgiorno et al., 2014) that, in low-grade pancreatic lesions of $p48^{cre}$;LSL-$Kras^{G12D}$ (KC) mice, DCLK1, acetylated α-tubulin, and β-endorphin mark the same population of cells (Figures S1A–S1D), and also found that these cells are negative for the intestine-derived Tuft cell marker POU2F3 (Figures S1E and S1F).

Y1068-phosphorylated EGFR is localized to the membrane in most PanIN cells (Figure 1A), but in $DCLK1^+$ PanIN cells it is primarily clustered in apical areas where it co-localizes with acetylated alpha-tubulin (Figures 1B and 1C). EGFR signaling is terminated by lysosomal downregulation (Brankatschk et al., 2012; Sousa et al., 2012; Vieira et al., 1996), which was functionally linked to acetylation of α-tubulin (Gao et al., 2010; Liu et al., 2012). Analyses of acetylated $\alpha\text{-tubulin}^+$ and $DCLK1^+$ cells showed an increased expression of the lysosomal marker LAMP-1 (Figure 1D), and this correlated with a decrease in downstream signaling to ERK1/2 in $DCLK1^+$ cells (analyses of pT202/pY204-ERK1/2; Figures 1E and 1F). This suggests that EGFR, although capable of autophosphorylation at Y1068, is targeted to the lysosomes, which prevents downstream signaling to MAPK in these cells.

Chemical inhibition of EGFR signaling increases the occurrence of $DCLK1^+$ cells *in vitro* and *in vivo*

In light of the above data indicating dysfunctional EGFR signaling in $DCLK1^+$ cells, we next tested if inhibition of EGFR signaling could lead to formation of these cells. Therefore, we treated KC mice at an age of 4 weeks with control or the EGFR inhibitor erlotinib over a time span of 8 weeks (Figure S2A). At the endpoint we did not observe significant changes in the abnormal tissue area (including lesions and stroma) (Figure S2B) or apoptotic cell death within lesion areas (Figure S2C). However, as expected, we observed a significant decrease in active (Y1068-phosphorylated) EGFR (Figure S2D), which correlated with a significant increase in $DCLK1^+$ cells within ADM/PanIN lesions (Figures 2A and 2B).

In order to test if inhibition of EGFR can indeed lead to an increase in the $DCLK1^+$ cell population within PanIN lesion cells, we used an organoid system. SM3 are non-transformed cells from duct-like PanIN cells derived from $Pdx1^{cre}$;$Kras^{G12D}$ mice (Agbunag et al., 2006) that can be propagated for 25–30 passages. SM3 cells in organoid culture form PanIN-like structures (Liou et al., 2017) that contain $DCLK1^+$ cells (Figure 2C). Flow cytometric separation of $DCLK1^-$ and $DCLK1^+$ cells in SM3 PanIN cells showed that the

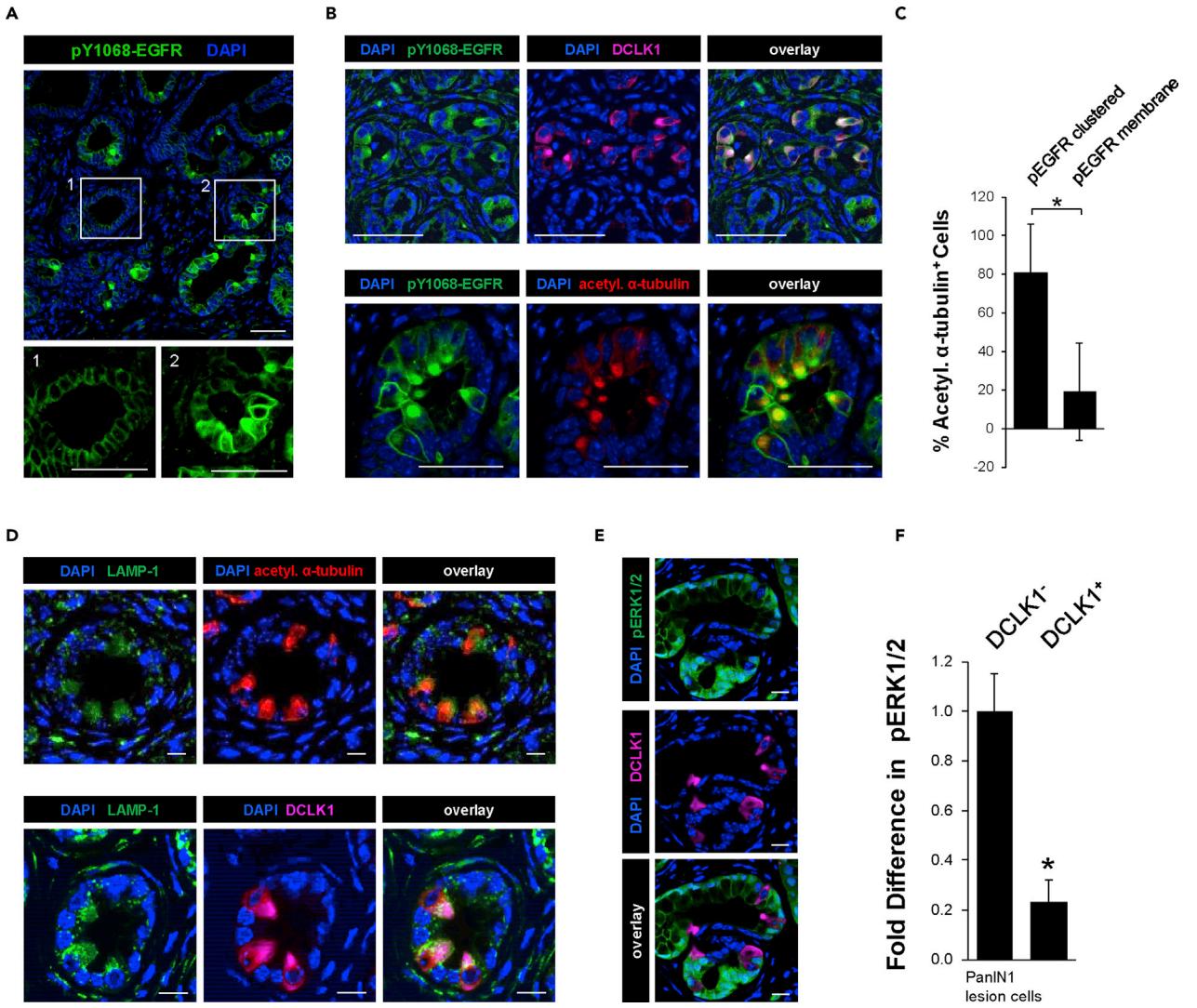

Figure 1. EGFR, although autophosphorylated, does not signal downstream to ERK1/2 in DCLK1$^+$ PanIN cells

(A) IHC-IF for pY1068-EGFR (green) and DAPI nuclear stain in p48^{cre};LSL-Kras^{G12D} (KC) mouse pancreas tissue. Scale bars indicate 50 μm.

(B) IHC-IF for pY1068-EGFR (green) and DCLK1 (pink; top) or acetylated α-tubulin (red; bottom) with DAPI nuclear stain in KC mouse pancreas tissue. Scale bars indicate 50 μm.

(C) Quantification of pY1068-EGFR signal in acetylated α-tubulin$^+$ PanIN cells (* indicates statistical significance; t test p value < 0.0001; n = 550 cells). Error bars indicate standard deviation.

(D) IHC-IF for LAMP-1 (green) and either acetylated α-tubulin (red; top) or DCLK1 (pink; bottom) with DAPI nuclear stain in KC mouse pancreas tissue. Scale bars indicate 10 μm.

(E) IHC-IF for pT202/pY204-ERK1/2 (labeled pERK1/2; green) and DCLK1 (pink) in KC mouse pancreas tissue. Scale bars indicate 50 μm.

(F) Quantification of pERK1/2 in DCLK1$^-$ or DCLK1$^+$ PanIN-1 lesion cells. Three mice were used to obtain the average fluorescent signal for pERK1/2 in DCLK1$^-$ or DCLK1$^+$ cells in ImageJ, represented as fold difference in the graph. Statistical significance, indicated by *, was determined using the paired t test; p value = 0.0064. Error bars represent the standard deviation.

DCLK1$^+$ population (8.75% ± 3.24% of cells in n = 3 replicates; Figure 2D) is also positive for the *in vivo* markers acetylated α-tubulin and β-endorphin (Figure S2E). Treatment of SM3 PanIN cells with erlotinib decreased EGFR activity, as measured by the presence of pERK1/2 (Figure S3A). Moreover, although fluorescence-activated cell sorting (FACS) analyses of SM3 PanIN cells treated with vehicle or erlotinib for 2 days did not significantly alter proliferation of DCLK1$^-$ or DCLK1$^+$ populations (Figure S3B), erlotinib did significantly increase the presence of DCLK1$^+$ cells (Figures 2E and 2F). Taken together, the data obtained with erlotinib support our finding that DCLK1$^+$ cells can develop owing to dysfunctional EGFR signaling.

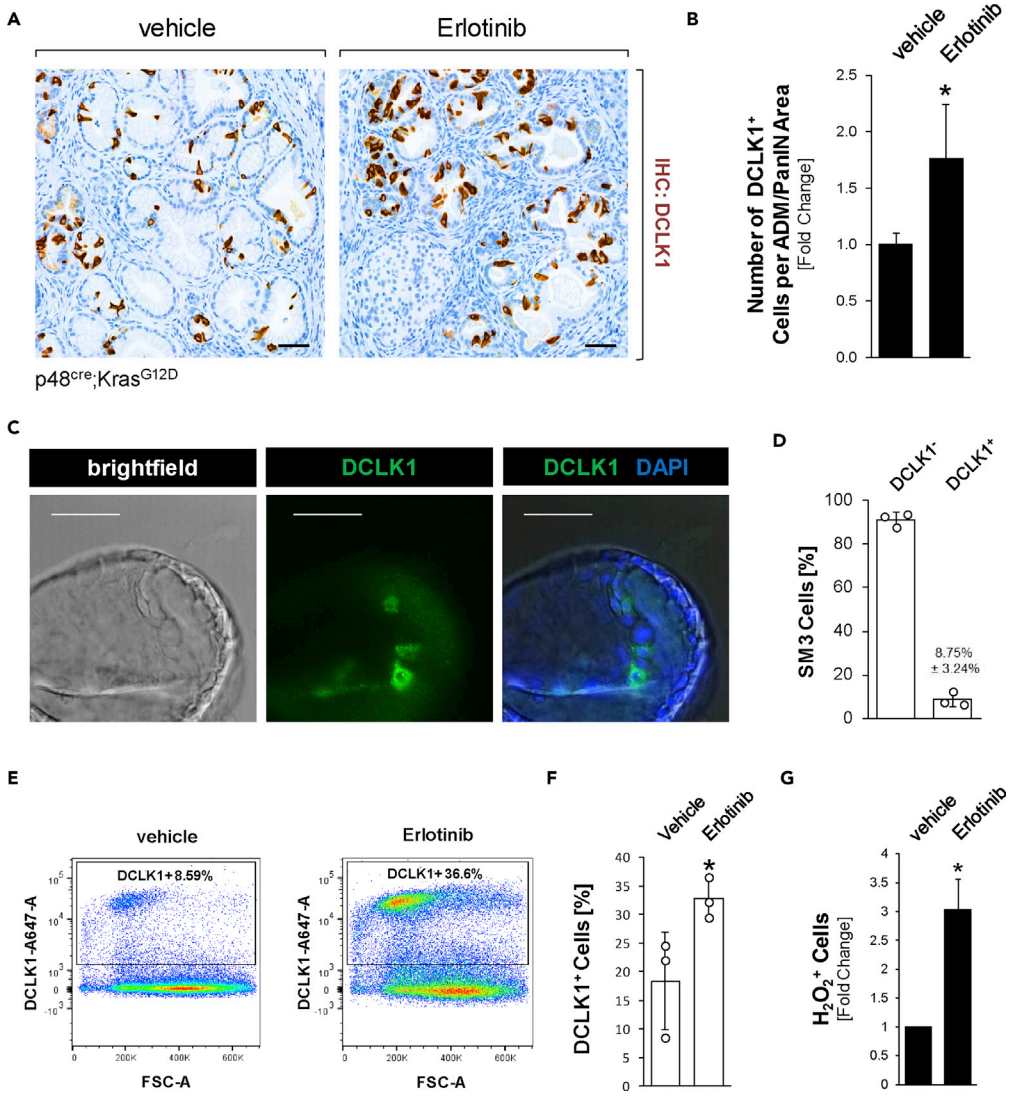

Figure 2. Chemical inhibition of EGFR signaling increases the occurrence of DCLK1$^+$ cells *in vitro* and *in vivo*

(A) IHC for DCLK1 in KC mice treated with vehicle or Erlotinib for 8 weeks. Scale bars indicate 50 μm.

(B) Quantification of the number of DCLK1$^+$ cells per ADM/PanIN lesion area, shown as fold change. Counting was done manually, and area measurements were done using Aperio ImageScope. Pancreata of n = 5 mice per treatment group were analyzed. Statistical significance, indicated by *, was determined using the t test; p value = 0.0071. Error bars indicate standard deviation.

(C) Imaging of brightfield, DAPI nuclear stain, and DCLK1 (green) immunofluorescence in SM3 cell PanIN organoids. Scale bars indicate 50 μm.

(D) Quantification of flow cytometry analysis of DCLK1$^-$ and DCLK1$^+$ SM3 cells, where the bars indicate the average of three experiments. Error bars indicate standard deviation.

(E) Representative plot of flow cytometry analysis of DCLK1 in control or erlotinib-treated SM3 cells.

(F) Quantification of flow cytometry in control or erlotinib-treated SM3 cells, where the bars indicate the average and * indicates statistical signficance (t test; p value = 0.05; n = 3). Error bars represent the standard deviation.

(G) Flow cytometry results from three independent experiments, using the Cell Meter Intracellular Fluorimetric Hydrogen Peroxide Assay Kit to measure intracellular hydrogen peroxide resulting from treatment of SM3 cells (n = 3 per group) with control or erlotinib (1 μM) for 2 days. Statistical significance, indicated by *, was determined using the paired t test; p value = 0.0224. Error bars represent the standard deviation.

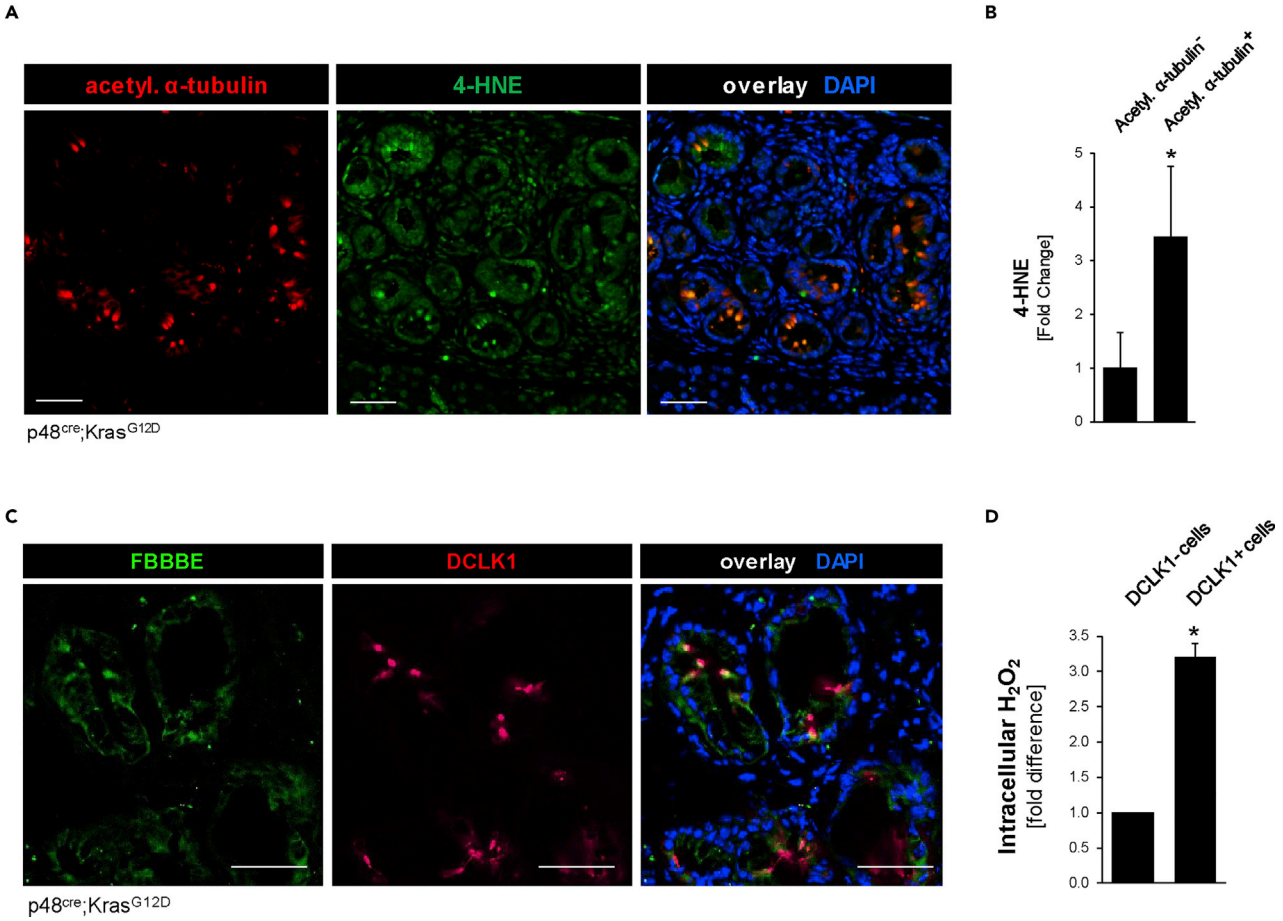

Figure 3. DCLK1$^+$ pancreatic lesion cells show increased hydrogen peroxide levels

(A) IHC-IF for acetylated α-tubulin (red) and 4-HNE (green) with DAPI nuclear stain in KC pancreas lesions. Scale bars indicate 50 μm.

(B) Quantification of 4-HNE in acetylated α-tubulin$^+$ and acetylated α-tubulin$^-$ lesion cells. Signal quantified in ImageJ and displayed as fold change (t test p value < 0.0001; n = 100 cells). * indicates statistical significance, and error bars represent standard deviation.

(C) Representative images of the fluorescent hydrogen peroxide sensor FBBBE (green) combined with DCLK1 (red) IHC-IF on fresh frozen KC mouse tissue. Scale bars indicate 50 μm.

(D) Quantification of the fluorescent FBBBE signal, indicating intracellular hydrogen peroxide, in DCLK1$^-$ and DCLK1$^+$ cells from pancreata of n = 3 mice. Signal quantified in ImageJ and displayed as fold change. Statistical significance, indicated by *, was determined using the t test; p value <0.0001. Error bars represent standard deviation.

DCLK1$^+$ pancreatic lesion cells show increased hydrogen peroxide levels

Inhibition of EGFR signaling previously has been shown to increase oxidative stress (Sobhakumari et al., 2013), and after treatment of SM3 PanIN cells with erlotinib we detected an approximately 3-fold increase in intracellular hydrogen peroxide (H_2O_2) (Figure 2G). Therefore, we next tested if oxidative stress levels are increased in the pancreatic DCLK1$^+$ and acetylated α-tubulin$^+$ cell population *in vivo*. Immunofluorescence-immunohistochemistry (IF-IHC) analyses of pancreatic lesion areas in KC mice indicated a significant increase in 4-HNE, a marker for intracellular oxidative stress, in the acetylated α-tubulin-positive cell population (Figures 3A and 3B). Moreover, specific probing for hydrogen peroxide (using FBBBE as a probe) showed a significant, over 3-fold increase in H_2O_2 in DCLK1$^+$ PanIN cells when compared with neighboring DCLK1$^-$ PanIN cells (Figures 3C and 3D).

PKD1 is highly expressed in DCLK1-positive pancreatic lesion cells and contributes to their abundance within lesions

Protein Kinase D1 is a kinase that is responsive to hydrogen peroxide (Doppler and Storz, 2007, 2017) and drives pancreatic lesion formation downstream of oncogenic KRas-induced oxidative stress (Liou et al., 2015, 2016). We therefore evaluated its expression and activity in the DCLK1$^+$ stem cell population. First,

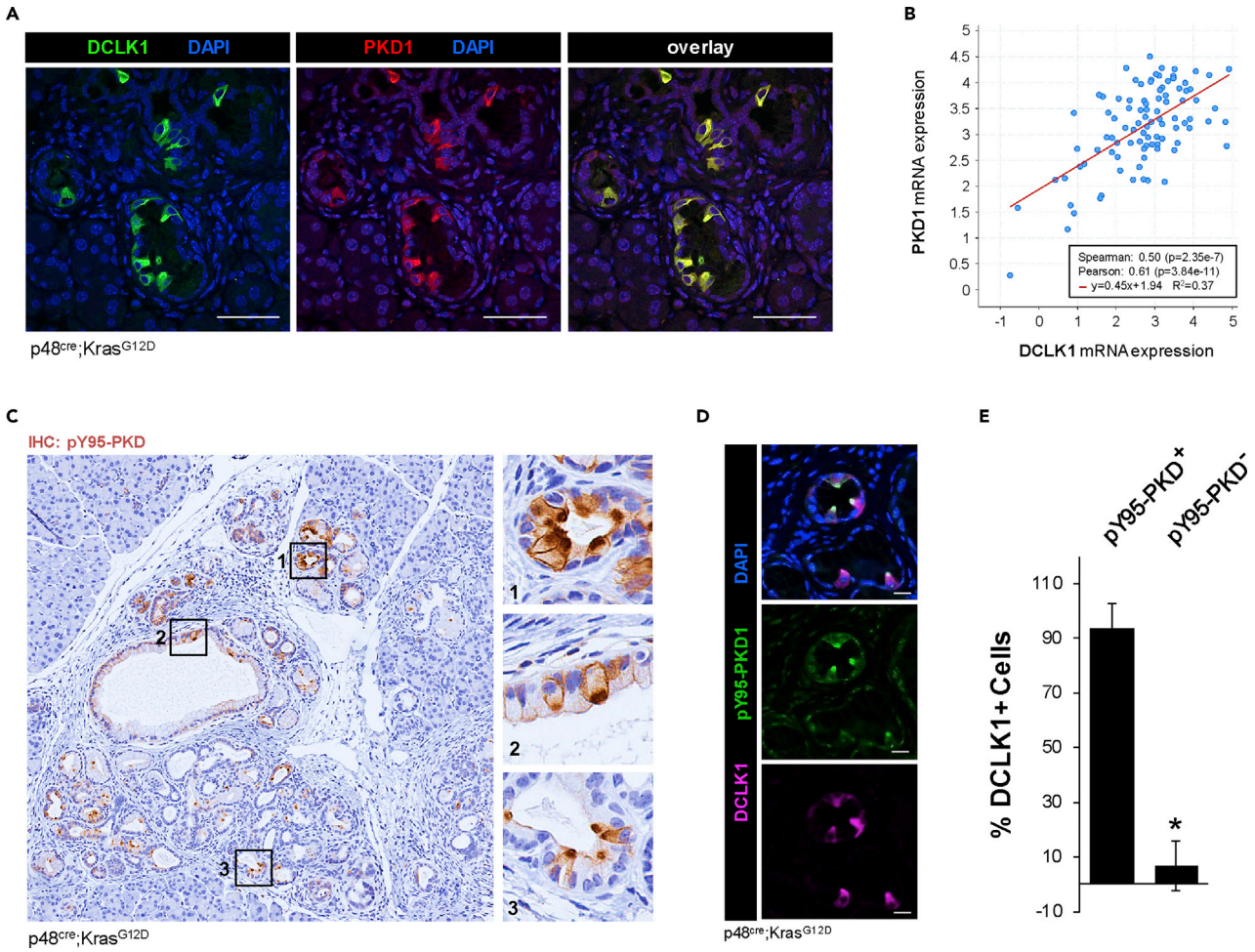

Figure 4. PKD1 is highly expressed in DCLK1-positive pancreatic lesion cells

(A) IHC-IF for DCLK1 (green) and PKD1 (red), with DAPI nuclear stain in KC mouse pancreas. The scale bars indicate 50 μm.

(B) PKD1 and DCLK1 mRNA expression data with regression line from https://www.cbioportal.org/ using the QCMG dataset containing 96 pancreatic adenocarcinoma samples.

(C) IHC for pY95-phosphorylated PKD in lesions of KC mice.

(D) IHC-IF for pY95-phosphorylated PKD (green) and DCLK1 (pink) in lesions of a KC mouse with DAPI nuclear stain. Scale bars represent 20 μm.

(E) Quantification of the percentage of DCLK1$^+$ cells with or without pY95-PKD (t test p value < 0.0001; n = 4 mice). * indicates statistical significance, and error bars represent standard deviation.

we found that PKD1 is highly expressed in DCLK1$^+$ cells of low-grade pancreatic lesions in KC mice (Figure 4A). Such a positive correlation of PKD1 and DCLK1 expression can also be detected in the QCMG patient dataset (Bailey et al., 2016), which contains mRNA expression data of 96 pancreatic adenocarcinoma samples (Figure 4B). Since DCLK1$^+$ cells show high levels of oxidative stress, we next probed for PKD1 phosphorylation at Y95, a residue whose phosphorylation was specifically linked to PKD activation by hydrogen peroxide (Doppler and Storz, 2007). We found that DCLK1$^+$ lesion cells showed an increase of Y95-phosphorylation of PKD1 (Figures 4C–4E), and this was confirmed by co-staining of pY95-PKD with acetylated α-tubulin$^+$ (Figure S4A).

We next analyzed our erlotinib-treated KC mice for expression of PKD1 and for ROS-activated PKD1 (as indicated by PKD phosphorylation at pY95). Both PKD1 expression and its ROS-induced tyrosine phosphorylation were significantly increased when mice were treated with erlotinib (Figures 5A–5C). A similar upregulation of PKD1 expression by erlotinib has been found in SM3 cells (Figure S4B). Overall, this supports our model that abrogation of proper EGFR signaling leads to increased expression and activity of PKD1.

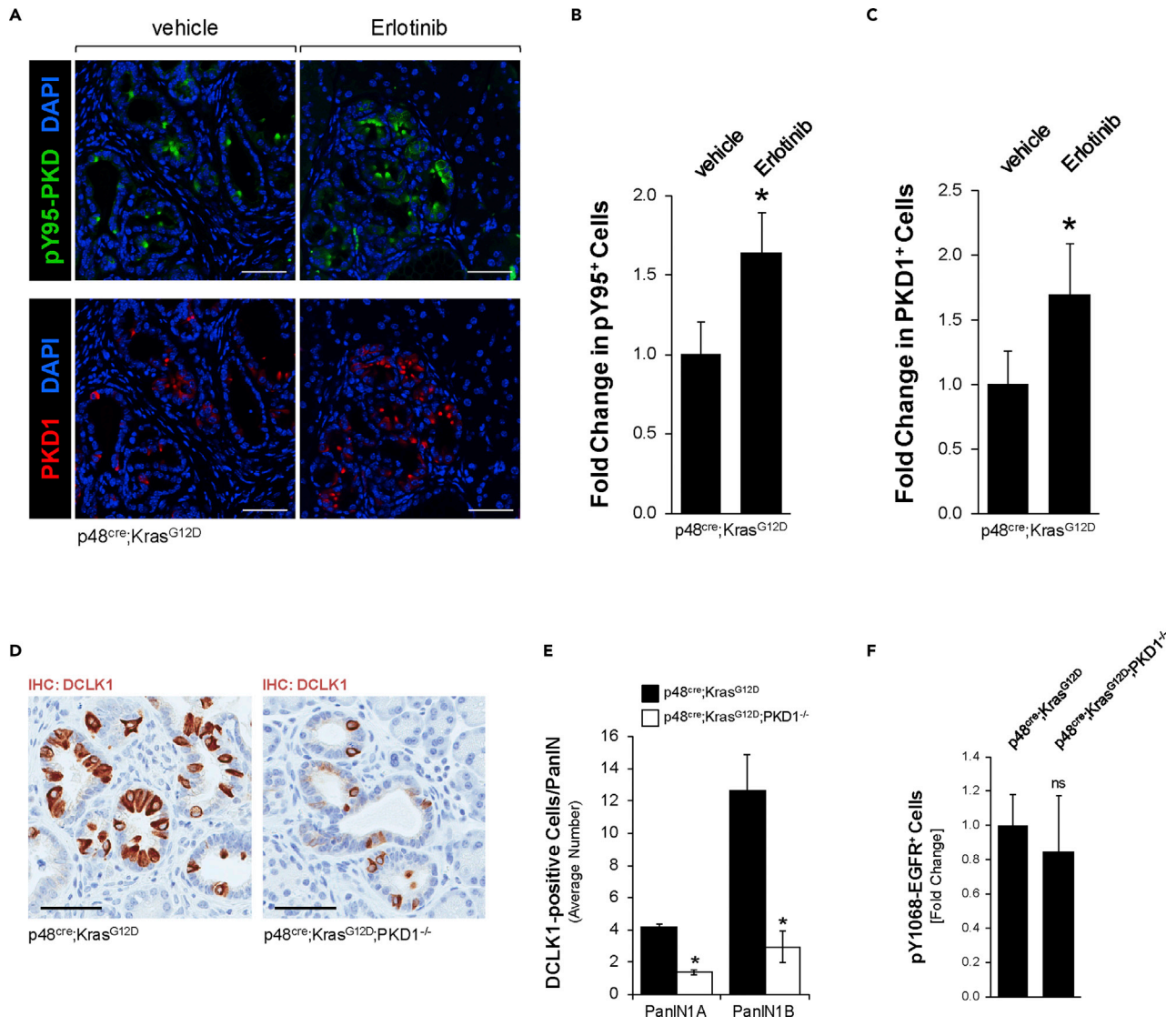

Figure 5. PKD1 contributes to the abundance of DCLK1-positive pancreatic lesion cells

(A) IHC-IF for pY95-PKD (green; top) or PKD1 (red; bottom), combined with DAPI nuclear stain in vehicle or erlotinib-treated KC mice. Scale bars indicate 50 μm.

(B) Quantification of pY95-PKD^{+} cells in vehicle or erlotinib treated KC mice. The number of pY95-PKD^{+} cells per lesion were counted and expressed as fold change (t test p value = 0.0079; n = 4 mice per group). * indicates statistical significance, and error bars represent standard deviation.

(C) Quantification of PKD1^{+} cells in vehicle or erlotinib-treated KC mice. The number of PKD1^{+} cells per lesion were counted and expressed as fold change (t test p value = 0.0256; n = 4 mice per group). * indicates statistical significance, and error bars represent standard deviation.

(D) Representative images of IHC for DCLK1 in KC and KC;PKD1$^{-/-}$ mice at 8 weeks of age. Scale bars indicate 50 μm.

(E) Quantification of DCLK1 IHC in PanIN-1 lesions of KC or KC;PKD1$^{-/-}$ mice (n = 4 pancreata per genotype). Statistical significance, indicated by *, was determined using the t test, p value <0.05. Error bars indicate standard deviation.

(F) Quantification of pY1068-EGFR in KC or KC;PKD1$^{-/-}$ mice. Signal was quantified in ImageJ and expressed as fold change (t test p value = 0.5206; n = 3 mice per group). Error bars represent standard deviation.

Eventually, we tested if oxidative stress-activated PKD1 is not only a marker for DCLK1^{+} cells but also a driving factor for the presence of these cells. Therefore, we compared KC mice with KC mice in which PKD1 is conditionally knocked out (p48^{cre};Kras^{G12D};PKD1$^{-/-}$) in pancreatic epithelial cells (described in Liou et al., 2015). We detected significantly fewer DCLK1^{+} cells in PanIN lesions from KC;PKD1$^{-/-}$ mice, when compared with PanIN lesions of KC mice (Figures 5D and 5E). As a control, demonstrating that PKD1 does not affect EGFR signaling, KC and KC;PKD$^{-/-}$ mice were analyzed for EGFR signaling. As expected, we found EGFR signaling (as determined by EGFR Y-1068-phosphorylation) unchanged between samples (Figure 5F).

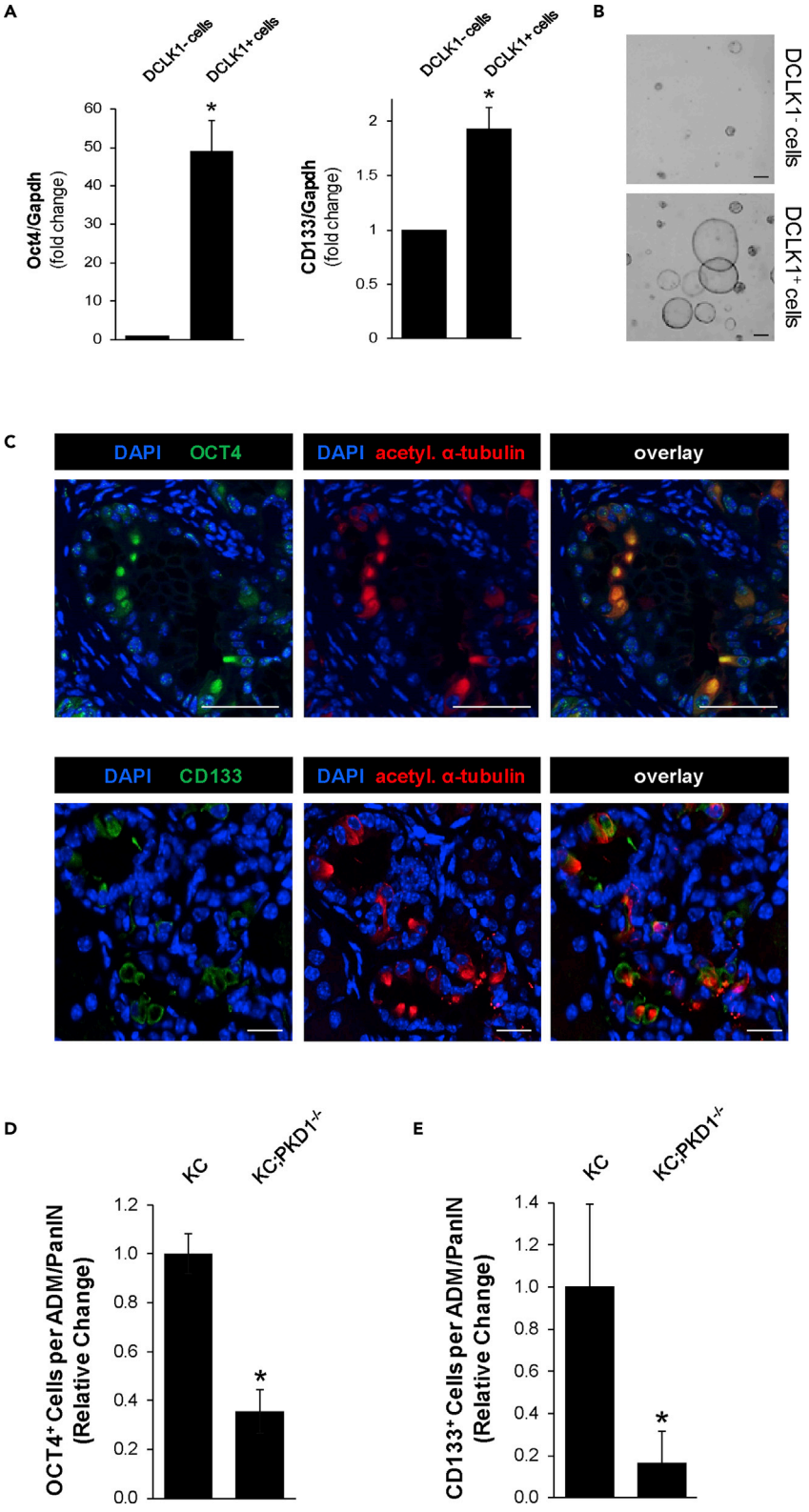
A
DCLK1- cells
DCLK1+ cells
Oct4/Gapdh
(fold change)
60
50
40
30
20
10
0
*
CD133/Gapdh
(fold change)
2
1.5
1
0.5
0
*
B
DCLK1- cells
DCLK1+ cells
C
DAPI OCT4
DAPI acetyl. α-tubulin
overlay
DAPI CD133
DAPI acetyl. α-tubulin
overlay
D
KC
KC;PKD1-/-
OCT4+ Cells per ADM/PanIN
(Relative Change)
1.2
1.0
0.8
0.6
0.4
0.2
0.0
*
E
KC
KC;PKD1-/-
CD133+ Cells per ADM/PanIN
(Relative Change)
1.4
1.2
1.0
0.8
0.6
0.4
0.2
0.0
*

Figure 6. DCLK1$^+$/acetylated α-tubulin$^+$ lesion cells express stem cell markers dependent on the presence of PKD1

(A and B) Primary cells from KC mouse pancreas were isolated and sorted for DCLK1. Sorted cells were analyzed via qPCR, where the graphs represent three replicates and the error bars represent the standard deviation. Statistical significance is indicated by *; the p value for Oct4 is 0.0005 and the p value for CD133 is 0.0014 (A). Sorted cells (10,000 per condition) were plated on top of Matrigel. Images represent day 5, and the scale bars indicate 200 μm (B).

(C) IHC-IF analysis of OCT4 (green) or CD133 (green) and acetylated α-tubulin (red) in KC mouse lesions. Scale bars indicate 50 μm (top panel, OCT4) and 20 μm (bottom panel, CD133).

(D) Quantification of OCT4 in lesions of 8-week-old KC (n = 4) and KC;PKD1$^{-/-}$ (n = 5) mice. Statistical significance , indicated by *, was determined by the t test; p value <0.0001.Error bars represent standard deviation.

(E) Quantification of CD133 in lesions of 8-week-old KC (n = 4) and KC;PKD1$^{-/-}$ (n = 4) mice. Statistical significance, indicated by *, was determined by the t test; p value = 0.0073. Error bars represent standard deviation.

DCLK1$^+$/acetylated α-tubulin$^+$ lesion cells express stem cell markers dependent on the presence of PKD1

The DCLK1$^+$ cell population previously has been discussed to have cancer stem cell properties (Bailey et al., 2014; Delgiorno et al., 2014). In order to verify that DCLK1$^+$ and PKD1$^+$ cells in low-grade lesions show stem cell characteristics, we sorted primary pancreatic cells from KC mice for DCLK1. As expected, the isolated DCLK1$^+$ cells expressed not only increased levels of DCLK1 and PKD1 (Figures S5A and S5B) but also increased levels of typical stem cell markers such as OCT4 and CD133 (Figure 6A). Moreover, DCLK1$^+$ cells formed PanIN-like structures when seeded in 3D culture, whereas DCLK1$^-$ cells, when seeded at the same number, were incapable of forming larger duct-like structures (Figure 6B). All PanIN-like ductal structures formed by DCLK1$^+$ cells were also positive for PKD1 (Figure S5C).

We then confirmed that the acetylated α-tubulin$^+$/DCLK1$^+$ pancreatic cancer cells in lesions of KC mice express these stem cell markers *in vivo*. Both OCT4 and CD133 were expressed in acetylated α-tubulin$^+$ cells (Figure 6C). Moreover, we detected a significantly decreased expression of both OCT4 and CD133 in PanIN lesions from KC;PKD1$^{-/-}$ mice, when compared with PanIN lesions of KC mice (Figures 6D, 6E, S5D, and S5E). Together this indicates that DCLK1$^+$ lesion cells express stem cell markers dependent on the presence of PKD1.

Ectopic expression of active PKD1 in PanIN cells increases the DCLK1$^+$ stem cell population

We next tested if ectopic expression of active PKD1 can increase the occurrence of DCLK1$^+$ stem cells. Flow cytometry analyses of SM3 PanIN cells indicated that all DCLK1$^+$ cells (5.98% for the experiment shown; 8.9% $\pm$ 4.3% in n = 5 replicates) were also positive for PKD1 (Figure 7A). This was confirmed by IF-IHC analyses of SM3 PanIN organoids, which also were positive for both markers (Figure 7B).

We then infected SM3 cells with a constitutively active version of human PKD1 (PKD1.S738E.S742E; PKD1.CA) and found that this increased the abundance of DCLK1$^+$ cells within the SM3 cell population (Figures 7C–7E). Analyses of a series of stem cell markers indicated that expression of PKD1.CA increased the expression of DCLK1, Pdx1, Notch1, Oct4, Satb2, Hes1, and CD133 stem cell population (Figure 7F). Together these data indicate that active PKD1 can be a driver of formation of DCLK1$^+$ stem cells in SM3 PanIN organoids, which supports the *in vivo* data seen in KC mice.

DISCUSSION

Pancreatic ductal adenocarcinoma is notoriously difficult to treat since it often is detected at a metastatic stage. Recent data suggest that cells that form metastases are seeded from low-grade dysplasia (ADM/PanIN) prior to the progression to cancer (Rhim et al., 2012). Expression of DCLK1 marks a subpopulation of PanIN cells that have been discussed as possible tumor and metastases initiating cells (Westphalen et al., 2016). DCLK1 is widely expressed on circulating tumor cells in serum from patients with stages I and II PDA (Qu et al., 2015), and DCLK1 expression was associated with a higher TNM stage and a higher rate of lymph node metastasis (Zhou et al., 2017). Considering evidence that the DCLK1$^+$ cell population plays a direct role in the aggressiveness of PDA, elucidating differences of these cells to other PanIN cells is key to finding targeted therapeutics.

Mouse models of PDA indicate that DCLK1$^+$ cells are most abundant in low-grade dysplasia (Bailey et al., 2014) but are distinct to Tuft cells, which also express DCLK1 but orchestrate inflammatory responses in

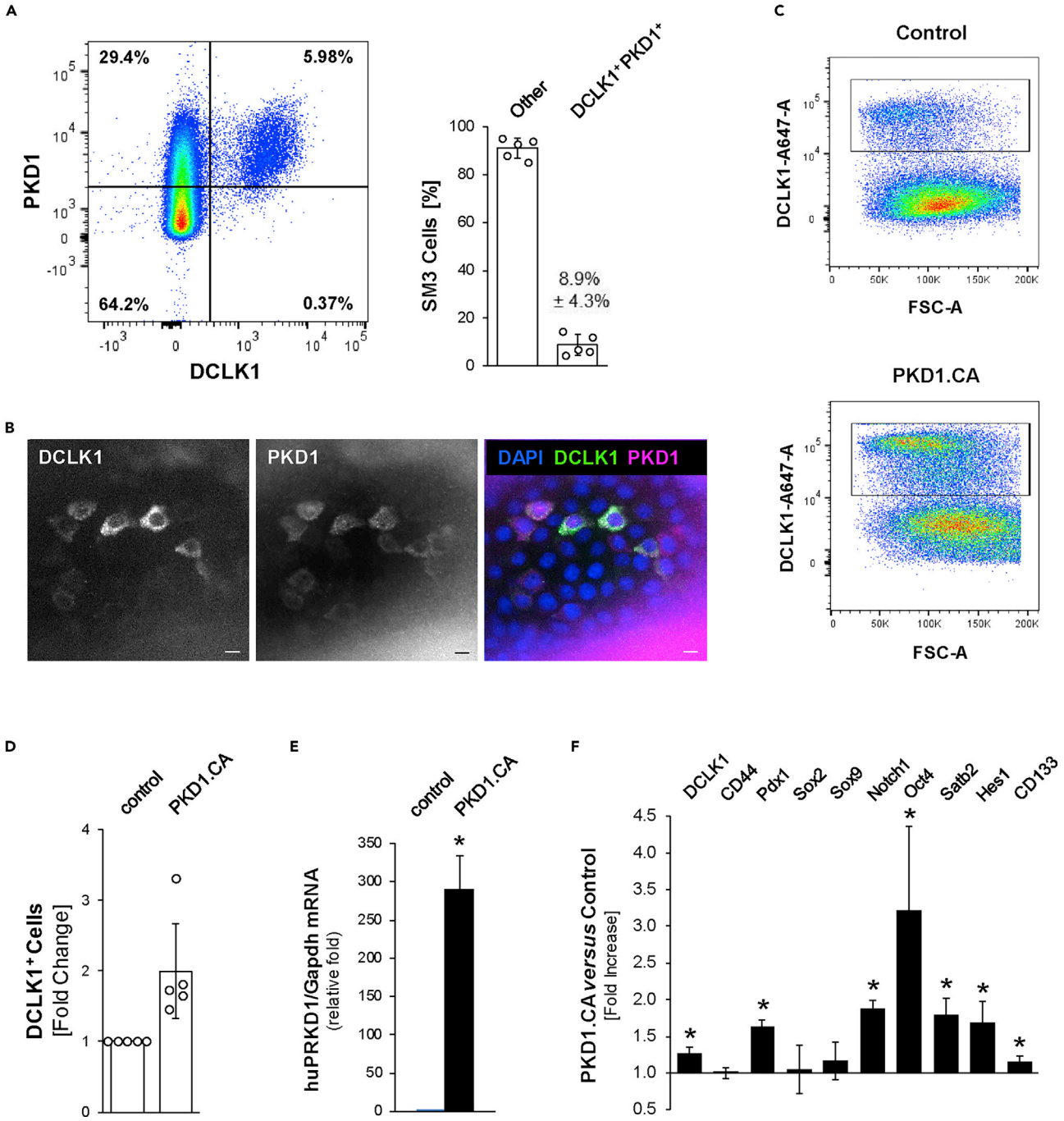

Figure 7. Ectopic expression of active PKD1 in PanIN cells increases the DCLK1$^+$ stem cell population

(A) Representative plot of flow cytometry analysis for cells positive for DCLK1 and PKD1 in SM3 PanIN cells (left); quantification of the percentage of SM3 cells that are DCLK1+ and PKD1$^+$ (right). "Other" indicates single positive cells or double-negative cells. Error bars indicate the standard deviation.

(B) Immunofluorescence for DCLK1 (green in overlay) and PKD1 (pink in overlay) in SM3 organoids with DAPI nuclear stain. Scale bars indicate 10 μm.

(C and D) Human constitutively active PKD1 (PKD1.CA) was overexpressed in mouse SM3 PanIN cells and flow cytometry analyses of cells for DCLK1 were performed. C shows representative flow cytometry plots. D shows quantification of flow cytometry analyses, where the graph indicates the fold change in DCLK1$^+$ cells from five independent experiments. Statistical significance, indicated by *, was determined by the paired t test; p value = 0.0205. Error bars represent the standard deviation.

(E) Quantitative PCR analysis for huPRKD1, to indicate overexpression of human constitutively active PKD1. Statistical significance is represented by * (t test; p value = 0.0003). Error bars indicate the standard deviation.

Figure 7. *Continued*

(F) Quantitative PCR analysis for expression of indicated genes and Gapdh (normalization) in SM3 cells overexpressing PKD1.CA versus control (n = 3 per condition). Statistical significance, indicated by *, was determined by the t test; DCLK1, p value = 0.0043; Pdx1, p value = 0.0003; Notch1, p value = 0.0002; Oct4, p value = 0.0279; Satb2, p value = 0.0040; Hes1, p value = 0.0135; CD133, p value = 0.0015. Error bars indicate the standard deviation.

glandular tissues (Gerbe et al., 2009; Gerbe and Jay, 2016; Howitt et al., 2016). Lineage tracing indicates that DCLK1$^+$ cells develop from PanIN cells by so far unidentified processes (Bailey et al., 2014). Here we show that DCLK1$^+$ cells have dysfunctional EGFR signaling and that this may act as a driver of formation of this cell population. In DCLK1$^-$ PanIN cells activated EGFR was detected at the cell membrane (Figure 1A), whereas in DCLK1$^+$ cells the activated receptor is clustered in the same apical region where acetylation of α-tubulin occurs (Figure 1B). Tubulin acetylation has been implicated in the regulation of dynamic transport processes within cells. For example, it promotes secretory vesicle flux and is required for efficient anterograde cargo transport (Dompierre et al., 2007; Reed et al., 2006). However, tubulin acetylation also was linked to premature delivery of EGFR vesicles to the degradative compartment, resulting in accelerated receptor degradation and downregulated signaling (Gao et al., 2010). Specifically, mitogenic signaling through ERK1/2 by the EGFR is attenuated by endocytosis and lysosomal degradation (Sousa et al., 2012). Both disturbance of vesicle trafficking and more rapid lysosomal progression may occur in DCLK1$^+$ cells, with the net effect of blocking efficient EGFR downstream signaling toward ERK1/2 (Figures 1E and 1F).

A downregulation of EGFR signaling as a driver of formation of DCLK1$^+$ PanIN cells is further supported by our data using erlotinib as a chemical inhibitor of EGFR. We indeed found that the DCLK1$^+$ cell population increased in response to erlotinib both *in vitro* (Figures 2E and 2F) and *in vivo* (Figures 2A and 2B), thereby providing further evidence that disruption of EGFR signaling is important in generating these PDA stem cells. Although erlotinib is approved for use with gemcitabine in patients with advanced pancreatic cancer owing to the increased 1-year survival rate of 23% (compared with 17% for gemcitabine + placebo) (Moore et al., 2007), patients with primarily resectable PDA gain no benefit from erlotinib (Sinn et al., 2017). Considering that the DCLK1$^+$ population is associated with poorer outcome (Nishio et al., 2017), and disrupting EGFR signaling increases the DCLK1$^+$ population, future studies could stratify patients to determine if erlotinib has different effectiveness in DCLK1-high versus DCLK1-low tumors.

Our data identify an increase in hydrogen peroxide as a potential driver of formation of DCLK1$^+$ PanIN cells (Figures 2G and 3A–3D). This increase may be due to dysfunctional EGFR signaling. It previously has been shown that inhibition of EGFR increases oxidative stress (Orcutt et al., 2011). Similarly, we found that erlotinib increased the formation of hydrogen peroxide in SM3 PanIN cells (Figure 2G). Moreover, increased levels of hydrogen peroxide have been shown to perturb signal transduction via endosomes (Kano et al., 2011), suggesting a potentiating effect on the downregulation of EGFR signaling. As a major target for increased levels of hydrogen peroxide we identified the oxidative stress-responsive kinase PKD1. In mouse pancreas PKD1 is not expressed in normal tissue but upregulated during the ADM process and during the formation of PanIN lesions (Liou et al., 2015) and, as we show here, highly expressed in DCLK1$^+$ cells (Figures 4A–4E). Moreover, comparison of low-grade dysplasia in KC mice to KC mice with a PKD1 knockout indicated that PKD1 may be a driver of occurrence of DCLK1$^+$ cells (Figures 5D and 5E).

We found that the expression of PKD1 in DCLK1$^+$ cells regulates the presence of stem cell markers such as CD133 and Oct4 (Figures 6D, 6E, and 7F). Notch, which regulates CD133 and CD133+ stem cell growth and metastasis (Kumar et al., 2016), previously has been implicated downstream of PKD1 (Liou et al., 2015). In addition, Oct4 together with Klf4 and Sox2 co-occupies the promoters of pluripotency-related genes (Evans et al., 2007; Wei et al., 2013). Thus, an increased expression of PKD1 and upregulation of its activity may be a key regulator of generation of DCLK1$^+$ stem cells. A role for another PKD isoform, PKD3, in tumor stemness recently has been shown for breast cancer (Lieb et al., 2020), further underlining a potential function for this kinase family in regulating tumor cell stemness.

In summary, the DCLK1$^+$ stem cell population plays a major role in PDA and understanding the differences between this cell type and other lesion cells can shed light on potential therapeutic approaches. With our findings that EGFR signaling is dysfunctional and not propagated to the nucleus and that oxidative stress/PKD1 signaling is increased, we identified key signaling events driving the formation of DCLK1$^+$ lesion cells. In future studies this knowledge can be exploited to target this pancreatic cancer stem cell population and to develop potential therapeutic approaches.

Limitations of the study

Although our study shows that disruption of EGFR signaling, increased oxidative stress, and PKD1 contribute to the occurrence of DCLK1^{+} cells in PanIN lesions, the study was often limited to murine tissue and primary cell culture. With the exception of Figure 4B, in which DCLK1 and PKD1 were shown to be correlated in PDA patient tissue, experiments were conducted in a precancerous murine model harboring a KrasG12D mutation. In addition, although this signaling is important in precancerous lesions, further studies are needed to understand the relevance to therapeutic approaches in patients. For example, erlotinib treatment in patients provided a modest increase in survival (Moore et al., 2007). In light of our study, combining erlotinib with DCLK1 inhibition may be efficacious. However, to address this, further studies are needed utilizing tumor models.

Resource availability

Lead contact

Further information and requests for resources and reagents should be directed to and will be fulfilled by the Lead Contact, Peter Storz (Storz.Peter@mayo.edu).

Materials availability

This study did not generate new unique reagents.

Data and code availability

This study did not generate unique datasets or code.

METHODS

All methods can be found in the accompanying Transparent methods supplemental file.

SUPPLEMENTAL INFORMATION

Supplemental Information can be found online at https://doi.org/10.1016/j.isci.2020.102019.

ACKNOWLEDGMENTS

The authors would like to thank Dr. Nabeel Bardeesy (Massachusetts General Hospital) for providing SM3 cells. We would like to acknowledge the support of Dr. Laura Lewis-Tuffin and the Cell and Tissue Analysis Shared Resource facility at Mayo Clinic in Florida for assistance with FACS analyses and our colleagues in the Storz laboratory for helpful discussions. We also thank the Champions for Hope (Funk-Zitiello Foundation) and Gary Chartrand Foundation for their continuous support. This work was supported by NIH grant CA200572 and the Mayo Clinic Cancer Center GI Cancer program (to P.S. and T.P.). The content is solely the responsibility of the authors and does not necessarily represent the official views of the National Cancer Institute or the National Institutes of Health. The funders had no role in study design, data collection and analysis, decision to publish, or preparation of the manuscript.

AUTHOR CONTRIBUTIONS

Conceived and designed the experiments: A.K.F.M., G.-Y.L., P.S. Performed the experiments: A.K.F.M., H.R.D., L.I.B., G.-Y.L., B.E. Analyzed the data: A.K.F.M., G.-Y.L., H.R.D., L.I.B., P.S. Contributed reagents and tools: M.L., T.P. Wrote the paper: A.K.F.M., P.S.

DECLARATION OF INTERESTS

The authors declare no competing interests.

Received: July 21, 2020
Revised: November 25, 2020
Accepted: December 29, 2020
Published: January 22, 2021

REFERENCES

Agbunag, C., Lee, K.E., Buontempo, S., and Bar-Sagi, D. (2006). Pancreatic duct epithelial cell isolation and cultivation in two-dimensional and three-dimensional culture systems. Methods Enzymol. *407*, 703–710.

Bailey, J.M., Alsina, J., Rasheed, Z.A., McAllister, F.M., Fu, Y.Y., Plentz, R., Zhang, H., Pasricha, P.J., Bardeesy, N., Matsui, W., et al. (2014). DCLK1 marks a morphologically distinct subpopulation of cells with stem cell properties in preinvasive pancreatic cancer. Gastroenterology *146*, 245–256.

Bailey, P., Chang, D.K., Nones, K., Johns, A.L., Patch, A.M., Gingras, M.C., Miller, D.K., Christ, A.N., Bruxner, T.J., Quinn, M.C., et al. (2016). Genomic analyses identify molecular subtypes of pancreatic cancer. Nature *531*, 47–52.

Brankatschk, B., Wichert, S.P., Johnson, S.D., Schaad, O., Rossner, M.J., and Gruenberg, J. (2012). Regulation of the EGF transcriptional response by endocytic sorting. Sci. Signal. *5*, ra21.

Delgiorno, K.E., Hall, J.C., Takeuchi, K.K., Pan, F.C., Halbrook, C.J., Washington, M.K., Olive, K.P., Spence, J.R., Sipos, B., Wright, C.V., et al. (2014). Identification and manipulation of biliary metaplasia in pancreatic tumors. Gastroenterology *146*, 233–244.e5.

Dompierre, J.P., Godin, J.D., Charrin, B.C., Cordelieres, F.P., King, S.J., Humbert, S., and Saudou, F. (2007). Histone deacetylase 6 inhibition compensates for the transport deficit in Huntington's disease by increasing tubulin acetylation. J. Neurosci. *27*, 3571–3583.

Doppler, H., and Storz, P. (2007). A novel tyrosine phosphorylation site in protein kinase D contributes to oxidative stress-mediated activation. J. Biol. Chem. *282*, 31873–31881.

Doppler, H., and Storz, P. (2017). Mitochondrial and oxidative stress-mediated activation of protein kinase D1 and its importance in pancreatic cancer. Front. Oncol. *7*, 41.

Evans, P.M., Zhang, W., Chen, X., Yang, J., Bhakat, K.K., and Liu, C. (2007). Kruppel-like factor 4 is acetylated by p300 and regulates gene transcription via modulation of histone acetylation. J. Biol. Chem. *282*, 33994–34002.

Gao, Y.S., Hubbert, C.C., and Yao, T.P. (2010). The microtubule-associated histone deacetylase 6 (HDAC6) regulates epidermal growth factor receptor (EGFR) endocytic trafficking and degradation. J. Biol. Chem. *285*, 11219–11226.

Gerbe, F., Brulin, B., Makrini, L., Legraverend, C., and Jay, P. (2009). DCAMKL-1 expression identifies Tuft cells rather than stem cells in the adult mouse intestinal epithelium. Gastroenterology *137*, 2179–2180, author reply 2180-2181.

Gerbe, F., and Jay, P. (2016). Intestinal tuft cells: epithelial sentinels linking luminal cues to the immune system. Mucosal Immunol. *9*, 1353–1359.

Gzil, A., Zarebska, I., Bursiewicz, W., Antosik, P., Grzanka, D., and Szylberg, L. (2019). Markers of pancreatic cancer stem cells and their clinical and therapeutic implications. Mol. Biol. Rep. *46*, 6629–6645.

Harvey, K.F., Zhang, X., and Thomas, D.M. (2013). The Hippo pathway and human cancer. Nat. Rev. Cancer *13*, 246–257.

Hermann, P.C., Huber, S.L., Herrler, T., Aicher, A., Ellwart, J.W., Guba, M., Bruns, C.J., and Heeschen, C. (2007). Distinct populations of cancer stem cells determine tumor growth and metastatic activity in human pancreatic cancer. Cell Stem Cell *1*, 313–323.

Hong, S.P., Wen, J., Bang, S., Park, S., and Song, S.Y. (2009). CD44-positive cells are responsible for gemcitabine resistance in pancreatic cancer cells. Int. J. Cancer *125*, 2323–2331.

Howitt, M.R., Lavoie, S., Michaud, M., Blum, A.M., Tran, S.V., Weinstock, J.V., Gallini, C.A., Redding, K., Margolskee, R.F., Osborne, L.C., et al. (2016). Tuft cells, taste-chemosensory cells, orchestrate parasite type 2 immunity in the gut. Science *351*, 1329–1333.

Kano, F., Arai, T., Matsuto, M., Hayashi, H., Sato, M., and Murata, M. (2011). Hydrogen peroxide depletes phosphatidylinositol-3-phosphate from endosomes in a p38 MAPK-dependent manner and perturbs endocytosis. Biochim. Biophys. Acta *1813*, 784–801.

Kumar, D., Kumar, S., Gorain, M., Tomar, D., Patil, H.S., Radharani, N.N.V., Kumar, T.V.S., Patil, T.V., Thulasiram, H.V., and Kundu, G.C. (2016). Notch1-MAPK signaling axis regulates CD133(+) cancer stem cell-mediated melanoma growth and angiogenesis. J. Invest. Dermatol. *136*, 2462–2474.

Li, C., Heidt, D.G., Dalerba, P., Burant, C.F., Zhang, L., Adsay, V., Wicha, M., Clarke, M.F., and Simeone, D.M. (2007). Identification of pancreatic cancer stem cells. Cancer Res. *67*, 1030–1037.

Lieb, W.S., Lungu, C., Tamas, R., Berreth, H., Rathert, P., Storz, P., Olayioye, M.A., and Hausser, A. (2020). The GEF-H1/PKD3 signaling pathway promotes the maintenance of triple-negative breast cancer stem cells. Int. J. Cancer *146*, 3423–3434.

Lin, P.T., Gleeson, J.G., Corbo, J.C., Flanagan, L., and Walsh, C.A. (2000). DCAMKL1 encodes a protein kinase with homology to doublecortin that regulates microtubule polymerization. J. Neurosci. *20*, 9152–9161.

Liou, G.Y., Bastea, L., Fleming, A., Doppler, H., Edenfield, B.H., Dawson, D.W., Zhang, L., Bardeesy, N., and Storz, P. (2017). The presence of interleukin-13 at pancreatic ADM/PanIN lesions alters macrophage populations and mediates pancreatic tumorigenesis. Cell Rep. *19*, 1322–1333.

Liou, G.Y., Doppler, H., Braun, U.B., Panayiotou, R., Scotti Buzhardt, M., Radisky, D.C., Crawford, H.C., Fields, A.P., Murray, N.R., Wang, Q.J., et al. (2015). Protein kinase D1 drives pancreatic acinar cell reprogramming and progression to intraepithelial neoplasia. Nat. Commun. *6*, 6200.

Liou, G.Y., Doppler, H., DelGiorno, K.E., Zhang, L., Leitges, M., Crawford, H.C., Murphy, M.P., and Storz, P. (2016). Mutant KRas-induced mitochondrial oxidative stress in acinar cells upregulates EGFR signaling to drive formation of pancreatic precancerous lesions. Cell Rep. *14*, 2325–2336.

Liu, W., Fan, L.X., Zhou, X., Sweeney, W.E., Jr., Avner, E.D., and Li, X. (2012). HDAC6 regulates epidermal growth factor receptor (EGFR) endocytic trafficking and degradation in renal epithelial cells. PLoS One *7*, e49418.

Moore, M.J., Goldstein, D., Hamm, J., Figer, A., Hecht, J.R., Gallinger, S., Au, H.J., Murawa, P., Walde, D., Wolff, R.A., et al. (2007). Erlotinib plus gemcitabine compared with gemcitabine alone in patients with advanced pancreatic cancer: a phase III trial of the National Cancer Institute of Canada Clinical Trials Group. J. Clin. Oncol. *25*, 1960–1966.

Nishio, K., Kimura, K., Amano, R., Nakata, B., Yamazoe, S., Ohira, G., Miura, K., Kametani, N., Tanaka, H., Muguruma, K., et al. (2017). Doublecortin and CaM kinase-like-1 as an independent prognostic factor in patients with resected pancreatic carcinoma. World J. Gastroenterol. *23*, 5764–5772.

Orcutt, K.P., Parsons, A.D., Sibenaller, Z.A., Scarbrough, P.M., Zhu, Y., Sobhakumari, A., Wilke, W.W., Kalen, A.L., Goswami, P., Miller, F.J., Jr., et al. (2011). Erlotinib-mediated inhibition of EGFR signaling induces metabolic oxidative stress through NOX4. Cancer Res. *71*, 3932–3940.

Qu, D., Johnson, J., Chandrakesan, P., Weygant, N., May, R., Aiello, N., Rhim, A., Zhao, L., Zheng, W., Lightfoot, S., et al. (2015). Doublecortin-like kinase 1 is elevated serologically in pancreatic ductal adenocarcinoma and widely expressed on circulating tumor cells. PLoS One *10*, e0118933.

Reed, N.A., Cai, D., Blasius, T.L., Jih, G.T., Meyhofer, E., Gaertig, J., and Verhey, K.J. (2006). Microtubule acetylation promotes kinesin-1 binding and transport. Curr. Biol. *16*, 2166–2172.

Rhim, A.D., Mirek, E.T., Aiello, N.M., Maitra, A., Bailey, J.M., McAllister, F., Reichert, M., Beatty, G.L., Rustgi, A.K., Vonderheide, R.H., et al. (2012). EMT and dissemination precede pancreatic tumor formation. Cell *148*, 349–361.

Siegel, R.L., Miller, K.D., and Jemal, A. (2020). Cancer statistics, 2020. CA Cancer J. Clin. *70*, 7–30.

Sinn, M., Bahra, M., Liersch, T., Gellert, K., Messmann, H., Bechstein, W., Waldschmidt, D., Jacobasch, L., Wilhelm, M., Rau, B.M., et al. (2017). CONKO-005: adjuvant chemotherapy with gemcitabine plus erlotinib versus gemcitabine alone in patients after R0 resection of pancreatic cancer: a multicenter randomized phase III trial. J. Clin. Oncol. *35*, 3330–3337.

Sobhakumari, A., Schickling, B.M., Love-Homan, L., Raeburn, A., Fletcher, E.V., Case, A.J., Domann, F.E., Miller, F.J., Jr., and Simons, A.L. (2013). NOX4 mediates cytoprotective autophagy induced by the EGFR inhibitor erlotinib in head and neck cancer cells. Toxicol. Appl. Pharmacol. *272*, 736–745.

Sousa, L.P., Lax, I., Shen, H., Ferguson, S.M., De Camilli, P., and Schlessinger, J. (2012). Suppression of EGFR endocytosis by dynamin depletion reveals that EGFR signaling occurs

primarily at the plasma membrane. Proc. Natl. Acad. Sci. U S A *109*, 4419–4424.

Sureban, S.M., May, R., Lightfoot, S.A., Hoskins, A.B., Lerner, M., Brackett, D.J., Postier, R.G., Ramanujam, R., Mohammed, A., Rao, C.V., et al. (2011). DCAMKL-1 regulates epithelial-mesenchymal transition in human pancreatic cells through a miR-200a-dependent mechanism. Cancer Res. *71*, 2328–2338.

Vieira, A.V., Lamaze, C., and Schmid, S.L. (1996). Control of EGF receptor signaling by clathrin-mediated endocytosis. Science *274*, 2086–2089.

Vinogradov, S., and Wei, X. (2012). Cancer stem cells and drug resistance: the potential of nanomedicine. Nanomedicine (Lond.) *7*, 597–615.

Wei, Z., Gao, F., Kim, S., Yang, H., Lyu, J., An, W., Wang, K., and Lu, W. (2013). Klf4 organizes long-range chromosomal interactions with the oct4 locus in reprogramming and pluripotency. Cell Stem Cell *13*, 36–47.

Westphalen, C.B., Takemoto, Y., Tanaka, T., Macchini, M., Jiang, Z., Renz, B.W., Chen, X., Ormanns, S., Nagar, K., Tailor, Y., et al. (2016). Dclk1 defines quiescent pancreatic progenitors that promote injury-induced regeneration and tumorigenesis. Cell Stem Cell *18*, 441–455.

Yan, R., Li, J., Zhou, Y., Yao, L., Sun, R., Xu, Y., Ge, Y., and An, G. (2020). Inhibition of DCLK1 down-regulates PD-L1 expression through Hippo pathway in human pancreatic cancer. Life Sci. *241*, 117150.

Zhou, B., Sun, C., Hu, X., Zhan, H., Zou, H., Feng, Y., Qiu, F., Zhang, S., Wu, L., and Zhang, B. (2017). MicroRNA-195 suppresses the progression of pancreatic cancer by targeting DCLK1. Cell. Physiol. Biochem. *44*, 1867–1881.

iScience, Volume *24*

Supplemental Information

Dysfunctional EGFR and oxidative stress-induced PKD1 signaling drive formation of DCLK1+ pancreatic stem cells

Alicia K. Fleming Martinez, Heike R. Döppler, Ligia I. Bastea, Brandy Edenfield, Tushar Patel, Michael Leitges, Geou-Yarh Liou, and Peter Storz

Supplemental Data Items

Figure S1, related to Figure 1

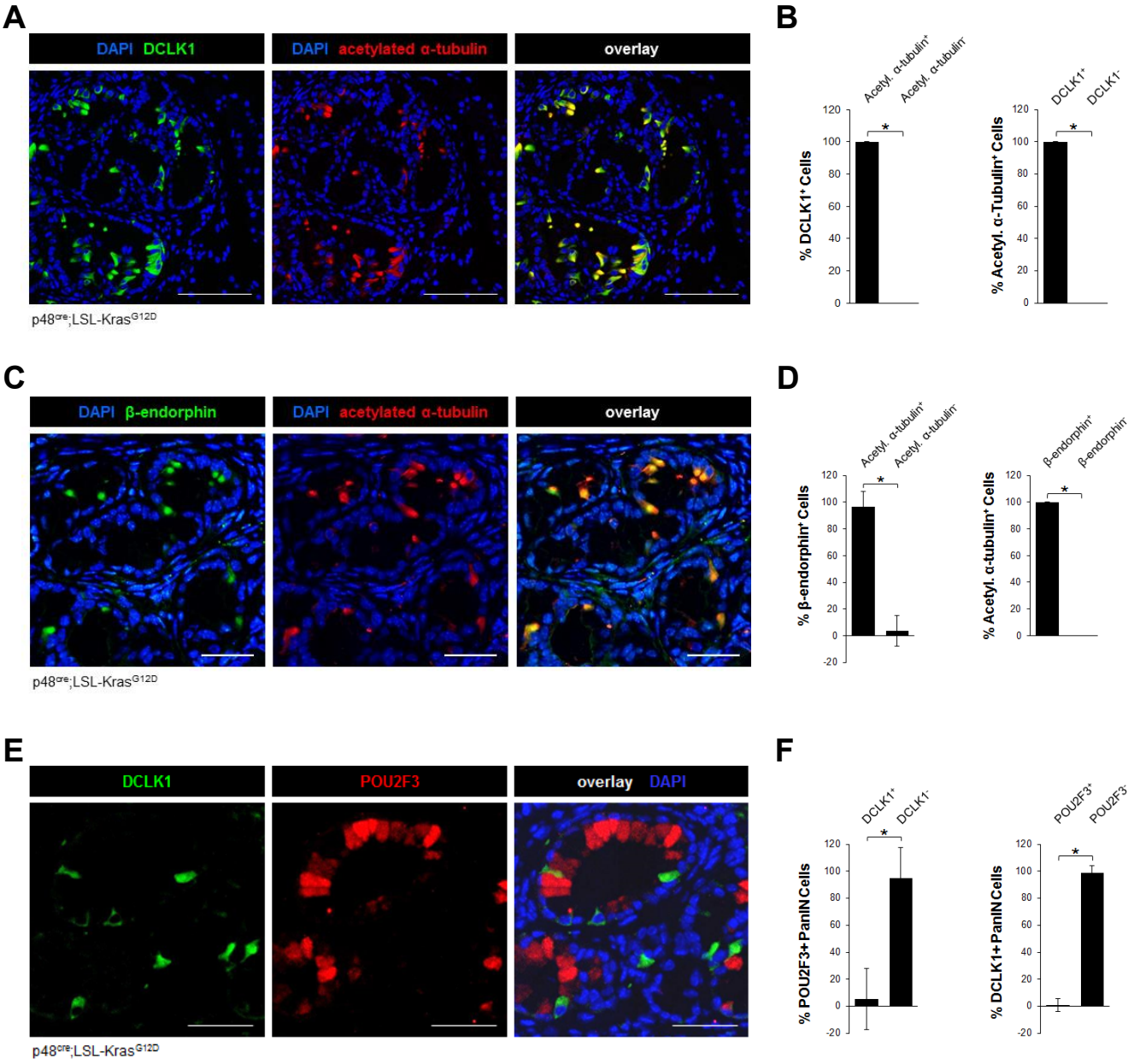

Supplemental Figure S1, related to Figure 1: **DCLK1⁺ cells in pancreatic lesions of KC mice are positive for acetylated α-tubulin and β-endorphin, but not for POU2F3. A, C, E:** Pancreatic lesions from 8 week old KC mice were stained for DCLK1 and acetylated α-tubulin (A), β-endorphin and acetylated α-tubulin (C), or DCLK1 and POU2F3 (E), as well as DAPI (nuclear stain). The scale bars indicate 100 μm (A) or 50 μm (C, E). **B:** Quantification of DCLK1 and acetylated α-tubulin in KC tissue, where there was 100% overlap (n =100 lesions). **D:** Quantification of β-endorphin and acetylated α-tubulin in KC tissue, where the p-value for the percentage of β-endorphin⁺ cells was <0.0001 and 100% of acetylated α-tubulin⁺ cells were β-endorphin⁺ (n = 77 lesions). **F:** Quantification of POU2F3 and DCLK1 in KC tissue, where the p-value for the percentage of POU2F3⁺ PanIN cells was <0.0001 and the p-value for the percentage of DCLK1⁺ PanIN cells was <0.0001 (n = 30 lesions).

Figure S2, related to Figure 2

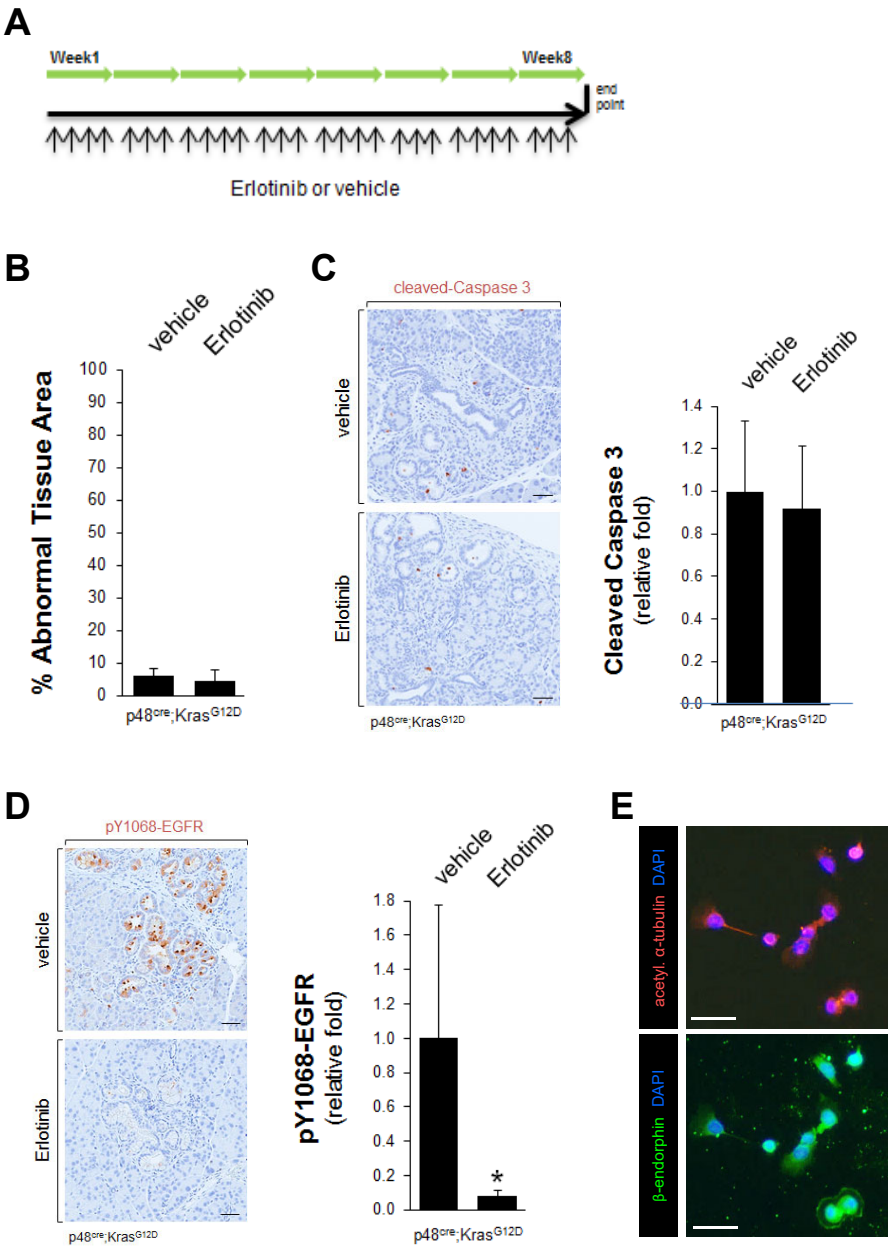

Supplemental Figure S2, related to Figure 2: A-D: **Erlotinib treatment in KC mice does not affect abnormal tissue area or apoptosis. A:** Schematic for Erlotinib treatment, given orally at 50mg/kg/day in MediGel Sucralose. **B:** Abnormal tissue (lesions plus stroma) area quantification for vehicle or Erlotinib treated KC mice. Tissue was manually outlined using Aperio ImageScope software (t-test p-value = 0.4059; n = 5 mice per group). **C:** Representative images and quantification of cleaved caspase-3 IHC in vehicle or Erlotinib treated KC mice. The positive pixel algorithm from Aperio was used to determine the fold change in brown IHC signal (t-test p-value = 0.6754; n = 5 mice per group). Scale bars indicate 50 μm. **D:** Representative images and quantification of pY1068-EGFR IHC in vehicle or Erlotinib treated KC mice. The positive pixel algorithm from Aperio was used to determine the fold change in brown IHC signal in 5 mice per group, where the p-value is 0.0290. Scale bars indicate 50 μm. **E:** Immunofluorescence for acetylated α-tubulin and β-endorphin in DCLK1^{+} cells sorted from the SM3 cell line. DAPI staining marks the nuclei. Scale bars indicate 50 μm.

Figure S3, related to Figure 3

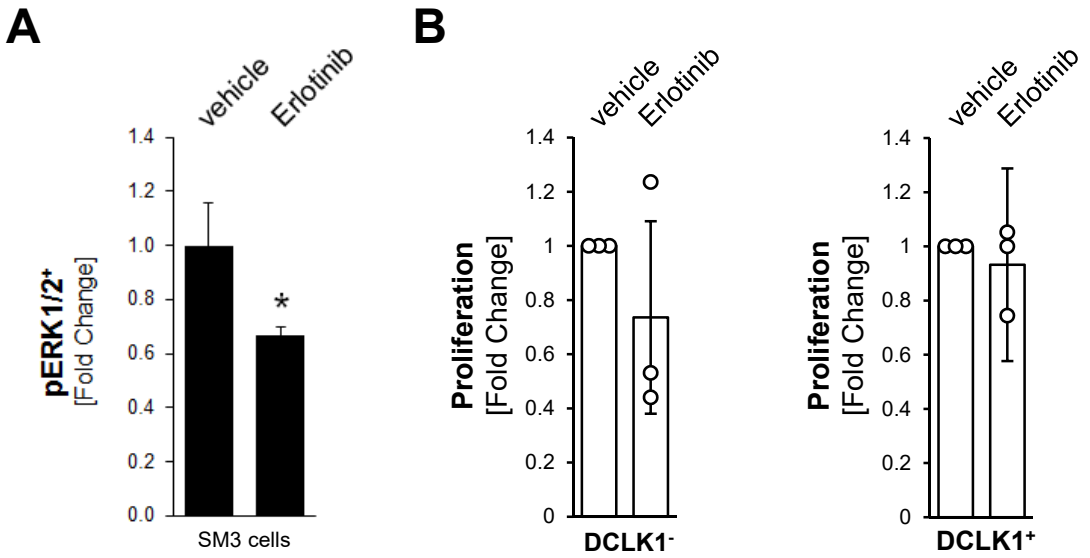

Supplemental Figure S3, related to Figure 3: **Erlotinib treatment in SM3 PanIN cells decreases pERK1/2 and does not affect proliferation. A:** Quantification of the percentage of pT202/pY204-ERK1/2^{+} SM3 cells, after two days of treatment with vehicle or 1μM Erlotinib. Bars represent the average of three repeats; p-value = 0.0207. **B:** Proliferation of sorted DCLK1^{-} or DCLK1^{+} SM3 cells after two days of vehicle or 1 μM Erlotinib treatment. Bars represent the average of three experiments, and the p-values are 0.3526 (DCLK1^{-}) and 0.5150 (DCLK1^{+}).

Figure S4, related to Figures 4 & 5

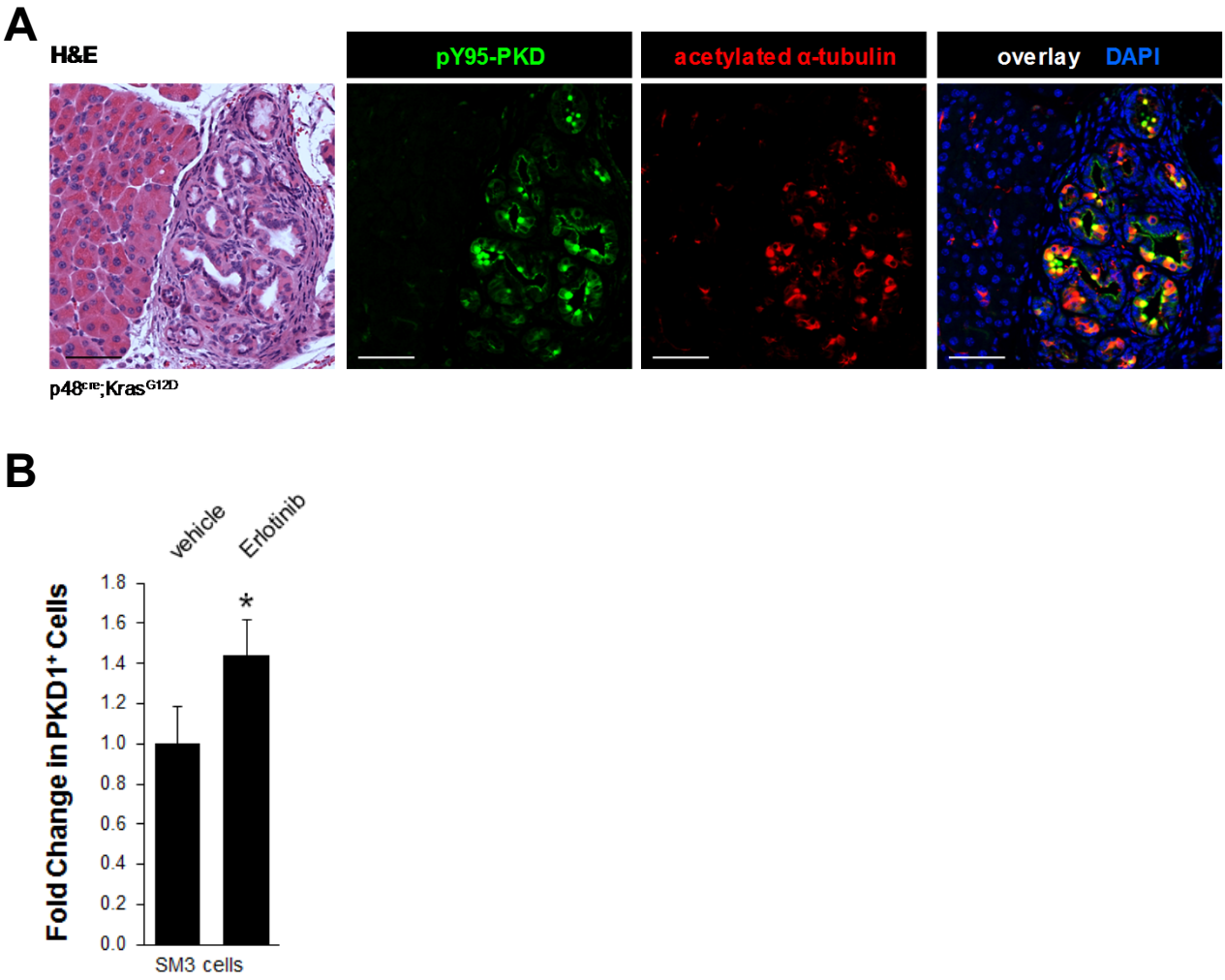

Supplemental Figure S4, related to Figures 4 & 5: **A: Acetylated α-tubulin-positive lesion cells are also positive for pY95-PKD.** Pancreatic lesions from 8 week old KC mice were stained by IF-IHC for pY95-PKD1 and acetylated α-tubulin, as well as DAPI (nuclear stain) and H&E. The scale bars indicate 50 μm. **B: Erlotinib treatment increases PKD1 expression.** Quantification of PKD1$^+$ SM3 PanIN cells after two days of vehicle or 1 μM Erlotinib treatment. Bars represent the average of 3 replicates; p-value = 0.0407.

Figure S5, related to Figure 5

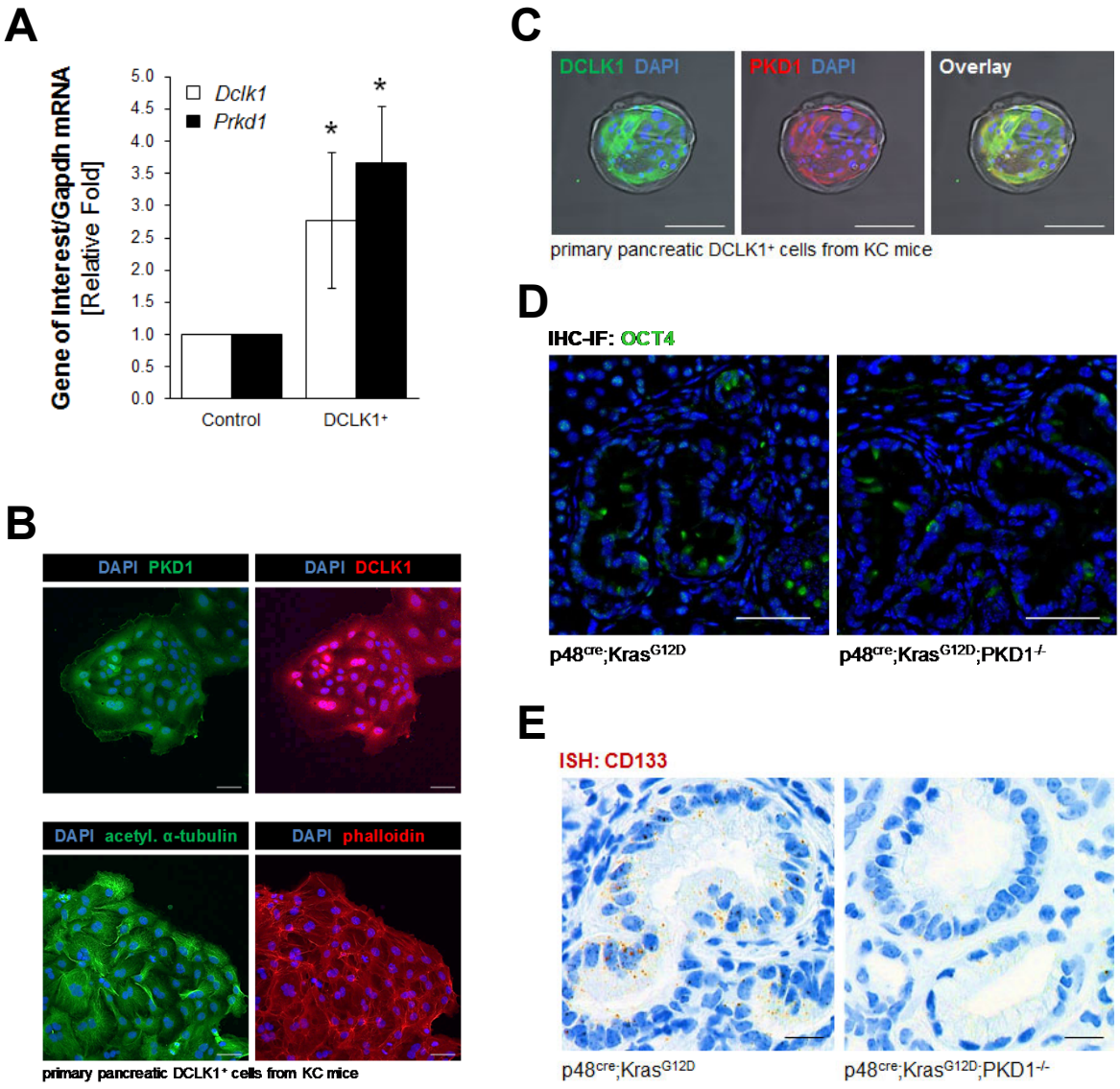

Supplemental Figure S5, related to Figure 5: **PKD1 is expressed in DCLK1⁺ cells, and knockout of PKD1 decreases stem cell markers Oct4 and CD133 in the KC mouse model. A:** qPCR for Dclk1 and Prkd1 in primary pancreatic DCLK1+ cells sorted from KC mice. Three replicates are graphed, and the p-values are 0.0440 for Dclk1 and 0.0065 for Prkd1. **B:** Immunofluorescence for PKD1, DCLK1, acetylated α-tubulin, and phalloidin in primary pancreatic DCLK1⁺ cells sorted from KC mice. Scale bars indicate 50 μm. **C:** Immunofluorescence for DCLK1 (green) and PKD1 (red) primary pancreatic DCLK1⁺ cells sorted from KC mice grown in Matrigel 3D culture. Scale bar indicates 100 μm. **D:** Immunofluorescence for OCT4 in KC or KC;PKD1$^{-/-}$ mouse tissue. Scale bars represent 50 μm. **E:** *In situ* hybridization for Prom1 (CD133) in KC or KC;PKD1$^{-/-}$ mouse tissue. Scale bars indicate 20 μm.

Supplementary Table S1

Antibody	Company/Source	Catalog Number	Species	IHC	IF	WB	FACS	IHC-IF Zenon
4-HNE	Alpha Diagnostic International	HNE12-S	goat	1:300				
acetylated α-tubulin	Sigma	T6793	mouse	1:2000	1:2000, 1:5000			
CD133	Proteintech	18470-1-AP	rabbit	1:1000				
cleaved Caspase-3	Cell Signaling Technologies	9661S	rabbit	1:100				
DCLK1	Abcam	ab37994	rabbit	1:250, 1:2000	1:250, 1:1000		1:50	1:340
DCLK1	R&D Systems	AF7138	sheep	1:250	1:250			
LAMP-1	Abcam	ab24170	rabbit	1:2000				
OCT4	Abcam	ab18976	rabbit	1:100				
PKD1	Abnova	H090005587-A01	mouse		1:200			
PKD1	Everest Biotech	EB12885	goat	1:500	1:500		1:200	
POU2F3	LifeSpan BioSciences	LS Bio C336168	rabbit					1:50
pT202/pY204-ERK1/2	Cell Signaling Technologies	4370S	rabbit	1:800	1:200			
pY1068-EGFR	Abcam	ab40815	rabbit	1:1000				
pY95-PKD	Storz Laboratory		rabbit	1:100				
β-endorphin	Immunostar	20063	rabbit	1:2000	1:2000			

Supplementary Table S1, Related to Figures 1-7 and Supplemental Figures S1-S5: **Antibodies and dilutions used.** Antibodies used were from the following sources: Abcam (Cambridge, MA), Abnova (Taipei, Taiwan), Alpha Diagnostic International (San Antonio, TX), Cell Signaling Technologies (Danvers, MA), Everest Biotech (Upper Heyford, Oxfordshire, UK), Immunostar (Hudson, WI), LifeSpan BioSciences (Seattle, WA), Proteintech (Rosemont, IL), R&D Systems (Minneapolis, MN), and Sigma (St. Louis, MO).

Transparent Methods

Cells, Antibodies and Reagents. SM3 PanIN cells were derived from Pdx1$^{cre/+}$; Kras$^{G12D/+}$ mice at six weeks of age, as previously described (Agbunag et al., 2006). Cells were maintained in DMEM/F-12 media with 15 mM HEPES (Gibco/ThermoFisher Scientific, Waltham, MA) with the following supplements: 5 mg/mL D-glucose (Sigma-Aldrich, St. Louis, MO), 1.22 mg/mL nicotinamide (Sigma-Aldrich), 5 nM 3,3,5-tri-iodo-L-thyronine (Sigma-Aldrich), 1 µM dexamethasone (Sigma-Aldrich), 100 ng/mL cholera toxin (Sigma), 5 mL/L insulin-transferrin-selenium + (Corning, Corning, NY), 100 U/mL penicillin-streptomycin (ThermoFisher Scientific), 0.1 mg/mL soybean trypsin inhibitor type 1 (Sigma-Aldrich), 20 ng/mL EGF (Peprotech, Rocky Hill, NJ), 5% NuSerum IV (Corning), 25 µg/mL bovine pituitary extract (Gibco/Thermo Scientific). All antibodies used for immunohistochemistry, immunofluorescence, and flow cytometry are detailed in **Supplemental Table S1**. 4′,6-Diamidino-2-phenylindole (DAPI) was from Sigma-Aldrich. Matrigel was from Corning (Corning, NY). Erlotinib was from SelleckChem (Houston, TX). FBBBE was from Cayman Chemical (Ann Arbor, MI). Collagenase I was from Millipore/Sigma (ST. Louis, MO).

Expression Constructs and Viral Transduction. For transfection, Lipofectamine 2000 (ThermoFisher Scientific, Waltham, MA) was used with the following constructs: pEGFP-N1 (Clontech, Mountain View, CA) or pEGFP-N1-PKD1.SS738/S742EE (Spratley et al., 2011). For lentiviral transduction, Lenti6.3/v5-GFP-PKD1.CA was generated by amplifying human PKD1.S738E.S742E using the following primers: 5′-CTGGATCCATGAGCGCCCCTCCGGTC-3′ and 5′-CCGCTCGAGTTACTTGTACAGCTCGTC-3′ and inserting the amplicon into pLenti6.3/V5-TOPO vector (Invitrogen, Carlsbad, CA) via TOPO cloning.

Mouse Lines and Treatment. Ptf1a/p48$^{cre/+}$, LSL-Kras$^{G12D/+}$ and LSL-PKD1$^{fl/fl}$ mouse strains, breeding of p48$^{cre/+}$;LSL-Kras$^{G12D/+}$ (KC) and p48$^{cre/+}$;LSL-Kras$^{G12D/+}$;LSL-PKD1$^{fl/fl}$ (KC;PKD1$^{-/-}$) mice and genotyping of mice have been described previously (Liou et al., 2015). Treatment with Erlotinib (or vehicle) began at 4 weeks of age and continued for 8 weeks as indicated in **Supplemental Figure S2A**. Erlotinib was dissolved in 5% DMSO, 30% PEG-300, 5% Tween-80, 60% water before being mixed into MediGel Sucralose (ClearH_2O, Portland, ME) and given every other day at 50 mg/kg/day per mouse. After 8 weeks of treatment, pancreata were collected and fixed in formalin for use in immunohistochemistry. With regards to gender, mice were randomly assigned to each treatment group, as we have not observed significant differences based on gender in the KC mouse model. All animal experiments were conducted under protocols (A30615 and A50214) approved by the Mayo Clinic Institutional Animal Care and Use Committee (IACUC) and were performed in accordance with relevant institutional and national guidelines and regulations.

Isolation of Primary Cells from KC Mice. The complete method for isolating primary pancreatic cells from KC mice has been described previously (Fleming Martinez and Storz, 2019). Briefly, resected tissue was dissociated at 37 ºC using 5 ml of 2 mg/mL collagenase (Sigma-Aldrich) in Hank's Balanced Salt Solution (HBSS; GE Healthcare, Chicago, IL). Tissue digestion was stopped by addition of cold HBSS and centrifugation at 931x g (4 ºC, 2 min). The cell pellet was then washed two times in cold HBSS with 5% FBS, sequentially put through a 500 µm mesh and a 105 µm mesh, and then added dropwise to a tube of 30% FBS in HBSS. After centrifugation (233x g, 4 ºC, 2 min), the cell pellet was used in flow cytometric analysis described below.

Flow Cytometric Analyses and Cell Sorting. Cells were labelled with Live/Dead Fixable Violet Dead Cell Stain Kit (ThermoFisher Scientific, 1 µL/1 million cells) for 30 min on ice in the dark; and then blocked using anti-CD32 (details in **Supplemental Table 1**) in HBSS + 1% BSA + 10% FBS. Following blocking, extracellular labelling was done (primary antibody 30 min on ice, washed, secondary antibody 30 min on ice). After washing, cells were fixed and permeabilized using Invitrogen's Fix & Perm Kit. Then, intracellular labelling was done (primary antibody 30 min on ice, washed, secondary antibody 30 min on ice). Cells were washed, filtered through a 40 µm filter (Fisher Scientific) to obtain a single cell suspension, and data was collected on the Attune NxT Flow Cytometer or cells were sorted on the BD FACS Aria II. Results from the Attune NxT were analyzed using FlowJo software. For cells analyzed with the Cell Meter Intracellular Fluorimetric Hydrogen Peroxide Assay Kit (AAT Bioquest), the Cell Meter dye was added to plates of cells per the manufacturer's protocol for 1 hour, washed off, and then cells were lifted with trypsin, washed, and re-suspended in HBSS + 10% FBS + 1% BSA. Once filtered (40 µm filter, Fisher Scientific), cells were put on the Attune NxT Flow Cytometer for data collection. Results were analyzed using FlowJo software.

Immunofluorescence. Cells were washed with PBS and then fixed in 4% paraformaldehyde in PBS for 15 min at 37 °C. After washing with PBS, cells were permeabilized (0.1% Triton X-100 in PBS, 2 min at room temperature) and then incubated with 100 mM glycerine in PBS for 2 min at room temperature. Cells were blocked with 3% BSA, 0.05% Tween in PBS and then incubated with primary antibodies overnight at 4 °C in blocking solution. After washing with PBS, cells were incubated with seconary antibodies (1:1000 in blocking solution, 2 hours at room temperature) and DAPI (1:10,000). After washing with PBS, ibidi Mounting Media (ibidi USA Inc., Fitchburg, WI) was added and cells were imaged using a LSM 510 (Zeiss, Oberkochen, Germany).

Immunohistochemistry (DAB and IF). Slides were deparaffinized and antigen retrieval was performed with 10 mM sodium citrate buffer (pH 6.0) for 25 min at 100°C. Samples were treated with 3% H_2O_2 (15 min, RT), rinsed with PBS and blocked (1 hr, RT) with serum-free Protein Block (DAKO, Santa Clara, CA). Then, hematoxylin and eosin (H&E) staining was performed or slides were incubated with primary antibodies (see **Supplemental Table 1**) diluted in Antibody Diluent Background Reducing Solution (Agilent, Santa Clara, CA). For DAB-IHC, EnVision Plus Anti-Rabbit Labelled Polymer Kit (Agilent) was used. For IF-IHC, slides were incubated with primary antibodies overnight, washed 3x for 5 min with 0.025% Tween-20 in PBS and then incubated with AlexaFluor488 or AlexaFluor647 labelled secondary antibodies (Invitrogen, Carlsbad, CA) at 1:500 (1 hr, RT) and DAPI (125 µg/ml; 10 min, RT). Slides were washed 3x with 0.025% Tween-20 in PBS and then mounted using PermaFluor Aqueous Mounting Medium (ThermoFisher Scientific, Waltham, MA). Images were captured using an Aperio ScanScope XT Scanner (Leica Biosystems, Buffalo Grove, IL), Aperio ScanScope FL Scanner (Aperio), or Pannoramic 250 FLASH III Scanner (3D Histech, Budapest, Hungary).

Immunofluorescence and FBBBE Analysis on Frozen Tissue Sections. Frozen tissue sections were fixed in ice-cold 95% ethanol for 15 min and then re-hydrated for 5 min at room temperature. Slides were incubated with 50 µM FBBBE for 1 hour at room temperature, rinsed in PBS, and then placed in 3% hydrogen peroxide shaking for 15 min at room temperature. After rinsing with PBS, slides were blocked for 1 hour at room temperature with serum-free Protein Block (DAKO, Santa Clara, CA) and rinsed again in PBS. Tissue was incubated with the primary antibody overnight at 4 °C, washed in PBS the next day, and then incubated with the secondary antibody for 2 hours at room temperature. Antibodies were diluted in Antibody Diluent Background Reducing Solution (Agilent, Santa Clara, CA). After washing with PBS, slides were coverslipped using PermaFluor Aqueous Mounting Medium (ThermoFisher Scientific, Waltham, MA).

***In Situ* Hybridization (ISH).** ISH was performed using RNAscope® Assay 2.5 HD Reagent Kit Brown (Advanced Cell Diagnostics, Hayward, CA) and is described in detail in (Bastea et al., 2019). Briefly, formalin-fixed, paraffin-embedded (FFPE) sections (5 µm) were baked (60°C, 1 hr), deparaffinized in xylene (15 min), dehydrated in 100% ethanol, and dried in a desiccator (RT, 12 hrs). Slides then were treated with H_2O_2 (10 min), followed by target retrieval (8 min) and protease treatment (15 min at 40°C in a hybridization oven). Next, slides were incubated with the indicated RNAscope target probe and amplification steps were according to the manufacturer's protocol. Slides were counterstained with hematoxylin, dehydrated and mounted.

Quantitative PCR. RNA was extracted using the RNeasy Plus Kit (Qiagen, Germantown, MD), and RNA was converted to cDNA using the High Capacity cDNA RT Kit (Applied Biosystems, Foster City, CA). Each qPCR reaction used Taqman Fast 2x PCR Mix (Applied Biosystems) and one of the following primer/probe sets (Applied Biosystems): mGapdh (Mm99999915_g1), mCd44 (Mm01277161_m1), mDclk1 (Mm00444950_m1), mHes1 (Mm01342805_m1), mNotch1 (Mm00435249_m1), mPdx1 (Mm00435565_m1), mPou5f1/OCT4 (Mm03053917_g1), mPrkd1 (Mm00435790_m1), hPrkd1 (Hs00177037_m1), mProm1/CD133 (Mm01211402_m1), mSatb2 (Mm00507331_m1), mSox2 (Mm03053810_s1) and mSox9 (Mm00448840_m1). Reactions were run on the QuantStudio 7 Flex Real-Time PCR System (Applied Biosystems). To calculate relative RNA abundance, the $\Delta\Delta C_T$ method was used with normalization to Gapdh.

CyQUANT Assay. After treatment, cells were washed with PBS before being frozen at -80 ºC. On the day of quantitation, plates were thawed at room temperature before 200 µL of CyQUANT® GR dye/cell-lysis buffer was added for 2-5 minutes in the dark. Fluorescence was then measured at 480 nm excitation and 520 nm emission on a BioTek Synergy HT plate reader.

Co-expression Analysis in Patient Samples. The QCMG patient data set (Bailey et al., 2016), consisting of mRNA expression data for 96 pancreatic adenocarcinoma samples was used (https://www.cbioportal.org) to generate a correlation coefficient for *PRKD1* and *DCLK1*.

Quantification and Statistical Analysis. All cell biological and biochemical experiments have been performed at least 3 times. For animal experiments, if not stated otherwise in the figure legends, at least 3 animals were used for quantification. Quantification was done by manual counting or by using the drawing tools in Aperio ImageScope (Leica Biosystems) to measure area in conjunction with manual counting. Quantification of immunofluorescence was done using ImageJ (U.S. National Institutes of Health, Bethesda, MD). The means are presented ± standard deviation. For statistical analysis, the p values were acquired using the unpaired t-test (unless specified otherwise in the figure legend) in GraphPad QuickCalcs (GraphPad Inc., La Jolla, CA). A two-tailed p value less than 0.05 was considered statistically significant.